Modeling and Experimental Studies of Mercury Oxidation and Adsorption in a Fixed-Bed Reactor

Topical Report

Reporting period: July 1, 2006 to March 31, 2009

Authors: Paula A. Buitrago, Mike Morrill, JoAnn S. Lighty, Geoffrey D. Silcox.

June 2009

DOE Award Number: DE-FC26-06NT42808
Tasks 5 and 6

University of Utah
Institute for Clean & Secure Energy
380 INSCC, 155 South, 1452 East
Salt Lake City, UT 84112

Disclaimer

ABSTRACT

This report presents experimental and modeling mercury oxidation and adsorption data. Fixed-bed and single-particle models of mercury adsorption were developed. The experimental data were obtained with two reactors: a 300-W, methane-fired, tubular, quartz-lined reactor for studying homogeneous oxidation reactions and a fixed-bed reactor, also of quartz, for studying heterogeneous reactions. The latter was attached to the exit of the former to provide realistic combustion gases. The fixed-bed reactor contained one gram of coconut-shell carbon and remained at a temperature of 150°C. All methane, air, SO_2, and halogen species were introduced through the burner to produce a radical pool representative of real combustion systems. A Tekran 2537A Analyzer coupled with a wet conditioning system provided speciated mercury concentrations. At 150°C and in the absence of HCl or HBr, the mercury uptake was about 20%. The addition of 50 ppm HCl caused complete capture of all elemental and oxidized mercury species. In the absence of halogens, SO_2 increased the mercury adsorption efficiency to up to 30 percent. The extent of adsorption decreased with increasing SO_2 concentration when halogens were present. Increasing the HCl concentration to 100 ppm lessened the effect of SO_2.

The fixed-bed model incorporates Langmuir adsorption kinetics and was developed to predict adsorption of elemental mercury and the effect of multiple flue gas components. This model neglects intraparticle diffusional resistances and is only applicable to pulverized carbon sorbents. It roughly describes experimental data from the literature. The current version includes the ability to account for competitive adsorption between mercury, SO_2, and NO_2.

The single particle model simulates in-flight sorbent capture of elemental mercury. This model was developed to include Langmuir and Freundlich isotherms, rate equations, sorbent feed rate, and intraparticle diffusion. The Freundlich isotherm more accurately described in-flight mercury capture. Using these parameters, very little intraparticle diffusion was evident. Consistent with other data, smaller particles resulted in higher mercury uptake due to available surface area. Therefore, it is important to capture the particle size distribution in the model. At typical full-scale sorbent feed rates, the calculations underpredicted adsorption, suggesting that wall effects can account for as much as 50 percent of the removal, making it an important factor in entrained-mercury adsorption models.

TABLE OF CONTENTS

EXECUTIVE SUMMARY

The heterogeneous mercury adsorption tests were completed in the fixed-bed reactor using activated carbon from coconut shells. The 1.2-cm-ID, quartz, fixed-bed reactor was connected to the existing, methane-fired tube furnace. The mean size of the carbon particles was 3 mm and the quartz frit that supports them was perforated with several 1-mm-diameter holes to reduce the pressure drop across the bed. For all tests the tubular reactor was operated with the high quench profile (440 K/s), an inlet mercury concentration of 25 $\mu g/m^3$, and a NO concentration of 20-30 ppm from the methane-fired burner.

The fixed-bed tests were performed at 150°C, 25 μg Hg/m^3, and included conditions with and without chlorine, bromine and SO_2. One gram of coconut-shell-based carbon was placed on the quartz frit. The thickness of the bed was about 2 cm and its temperature was controlled at 150°C. The presence of chlorine (50 ppm as HCl equivalent) dramatically increased mercury adsorption by the carbon, although the efficiency of the bed was reduced from 95 percent to 50 percent in the presence of 500 ppm SO_2. This reduction is no longer observed when the HCl concentration is increased to 100 ppm.

The addition of SO_2 also caused an increase in mercury adsorption by the carbon, although the extent of this increase was small compared to that obtained with HCl alone. The efficiency of mercury adsorption by the carbon in the presence of SO_2 was enhanced considerably when chlorine was added to the system.

Tests completed with bromine (35 ppm as HBr equivalent) showed an increase in mercury uptake by the carbon, similar to that obtained with HCl alone. No significant effect on the extent of adsorption was observed when either HCl, SO_2 or both were added to the system.

Preliminary adsorption tests made with 20 ppm of NO_2, in the absence of halogens, showed no effect on mercury adsorption. In the presence of NO_2 alone the carbon bed captured no elemental mercury at 150°C.

Modeling efforts focused on predicting mercury uptake for both a packed-bed and entrained-flow reactors. The packed-bed model is based on the Langmuir isotherm, neglects intraparticle diffusion resistances and is only applicable to pulverized-carbon sorbents. It roughly describes experimental data from the literature including the competitive effect between different flue gas components such SO_2 and NO_2.

The entrained-flow model for in-flight mercury capture was used to examine the suitability of the Langmuir and the Freundlich isotherms. Using parameters from a full-scale test, the Freundlich was better able to predict in-flight capture; little

intraparticle diffusional resistance was found with steep gradients near the particle surface. The model was used to help define the relative importance of in-flight capture and capture by sorbent on duct walls. Smaller particles, which result in more accessible surface area, showed more mercury uptake because of lower intraparticle diffusional resistance. Therefore, it is important to include particle size distribution in the model. In this study, this was accomplished by “binning” the particle sizes.

EXPERIMENTAL METHODS

The homogeneous mercury reactor used in this study is a 50-mm OD x 47-mm ID quartz tube (132 cm in length) located along the center of a high-temperature Thermcraft heater. The reaction tube extends 79 cm below the heater, is temperature controlled, and has a quartz sample section attached at the bottom with a capped end [1]. Peak gas temperature in the electrically heated zone was about 1080°C.

A methane-fired, premixed burner made of quartz glass supplied realistic combustion gasses to the reactor. All reactants were introduced through the burner and passed through the flame to create a radical pool representative of real combustion systems. The design burner heat input was about 300-W, producing 3.7 SLMP of combustion gases.

The heterogeneous tests were performed in the fixed bed reactor using activated carbon from coconut shells. The 1.2-cm-ID, quartz, fixed-bed reactor was connected to the existing, methane-fired tube furnace. The mean size of the carbon particles was 3 mm and the quartz frit that supported them was perforated with several 1-mm-diameter holes to reduce the pressure drop across the bed. The tests were conducted by loading the heterogeneous reactor with carbon, wrapping it with heating tape and insulation, and regulating the temperature to 150°C.

For all the tests, the tubular reactor was operated with the high quench profile (440 K/s) and an inlet mercury concentration of 25 $\mu g/m^3$. One gram of coconut-shell-based carbon was placed on the quartz frit. The thickness of the bed was about 2 cm. Initially, a mercury mass balance was closed with the homogeneous reactor in order to check the mercury concentrations entering the packed bed. The flue gases were then allowed to enter the heterogeneous reactor to study the effect of the sorbent. The baseline composition for all tests was: 25 ug/m^3 Hg, 0.88% O_2, 33 ppmv NO, 10.5 % CO_2, 9 ppmv CO.

To study the effects of other flue gas components such as SO_2, NO, NO_2, HCl, and HBr, different concentrations of these species were added to the baseline flue gas. All were introduced through the burner.

A Tekran 2537A mercury analyzer coupled with a wet sample conditioning system designed by Southern Research Institute (SRI) provided measurement of total and elemental mercury in the exhaust gas. In this system sample gas was pulled in two streams from the last section of the quartz reaction tube into a set of conditioning impingers. One stream was bubbled through a solution of stannous chloride to reduce the oxidized mercury to elemental form and then through a solution of sodium hydroxide to remove acid gases. This stream represented the total mercury concentration in the reactor. The second stream was first treated

with a solution of potassium chloride to remove oxidized mercury species and then was treated with a caustic solution for acid gas removal. This stream was representative of the elemental mercury concentration in the reactor. Oxidized species were calculated by the difference between total and elemental mercury concentrations. A chiller removed water from the sample gas and then each stream was intermittently sent to the analyzer [1] .

RESULTS AND DISCUSSION

Experimental Results

Due to the high pressure drop developed through the reactor it was not possible to use powdered activated carbon. Particles of larger size were used. Besides the particle size difference, the adsorption capacity of the coconut-shell carbon is typically higher than that for a coal-based carbon. The key factor affecting the adsorptive capacity of the bed is the sample size. One gram of carbon was used here and the large sample size is the reason that breakthrough curves were not observed in the periods of time considered.

Figure 1 shows the effects of starting the fixed bed adsorption process with 50 ppm chlorine (as HCl equivalent) and then adding increasing amounts of SO_2. Of most interest in Figure 1 is the almost complete lack of mercury adsorption when chlorine is absent at 150°C. The addition of SO_2 causes significant reductions in the amount of mercury adsorbed. The extent of the reduction is roughly proportional to the SO_2 concentration.

However, when the chlorine concentration is increased from 50 ppm to 100 ppm, as shown in Figure 2, the effect of SO_2 becomes negligible at concentrations ranging from 100 to 500 ppm. The order of injection for SO_2 and HCl also seems to play some role in the extent of mercury adsorption by the carbon. As shown in Figure 3, the addition of 50 ppm HCl at different SO_2 concentrations always results in an increase of the mercury uptake by the carbon; this increase is again nearly proportional to the SO_2 concentration. The SO_2 interferes with the ability of the carbon to adsorb mercury.

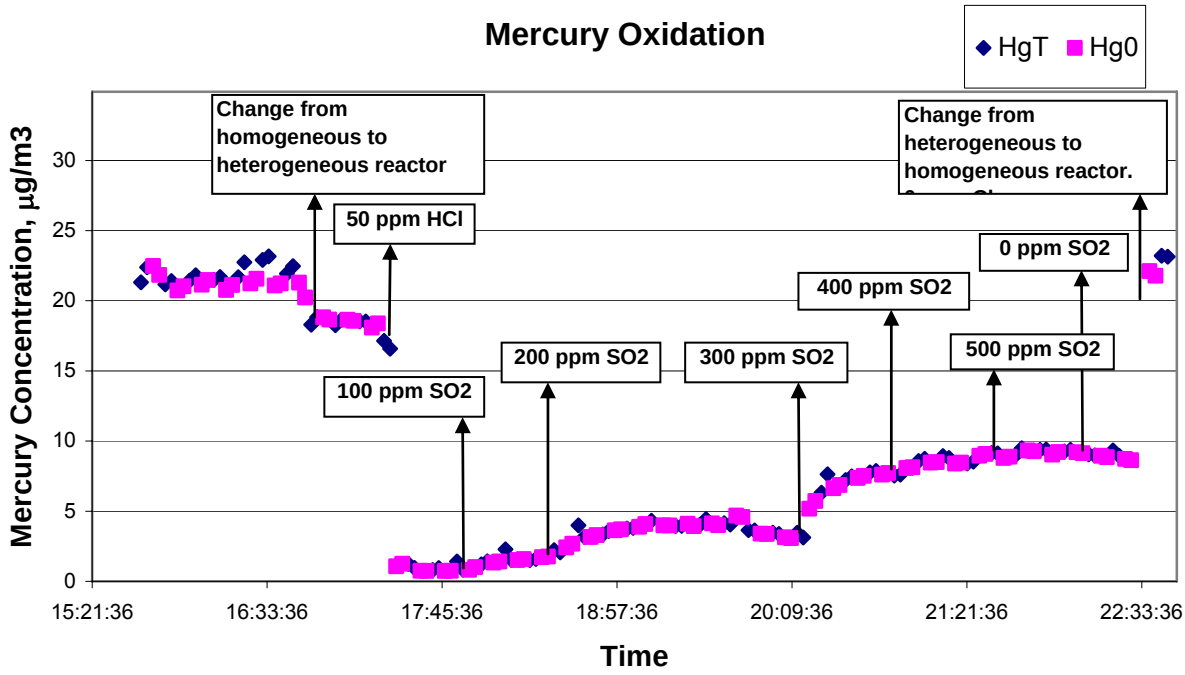

Figure 1 Elemental (Hg^0) and total (Hg^T) mercury concentrations at the exit of the carbon bed as a function of time (hours) at a temperature of 150°C at chlorine concentrations of 50 ppm (as HCl equivalent) and SO_2 concentrations ranging from 100 to 500 ppm.

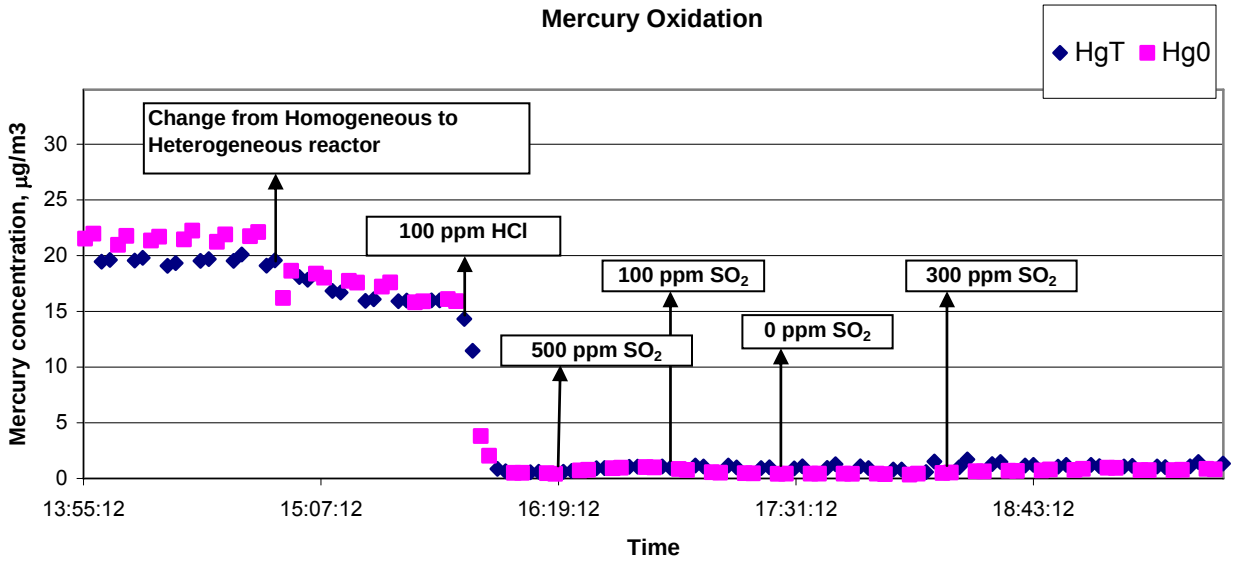

Figure 2 Elemental (Hg^0) and total (Hg^T) mercury concentrations at the exit of the carbon bed as a function of time (hours) at a temperature of 150°C at chlorine concentration of 100 ppm (as HCl equivalent) and SO_2 concentrations of 500, 100, and 300 ppm.

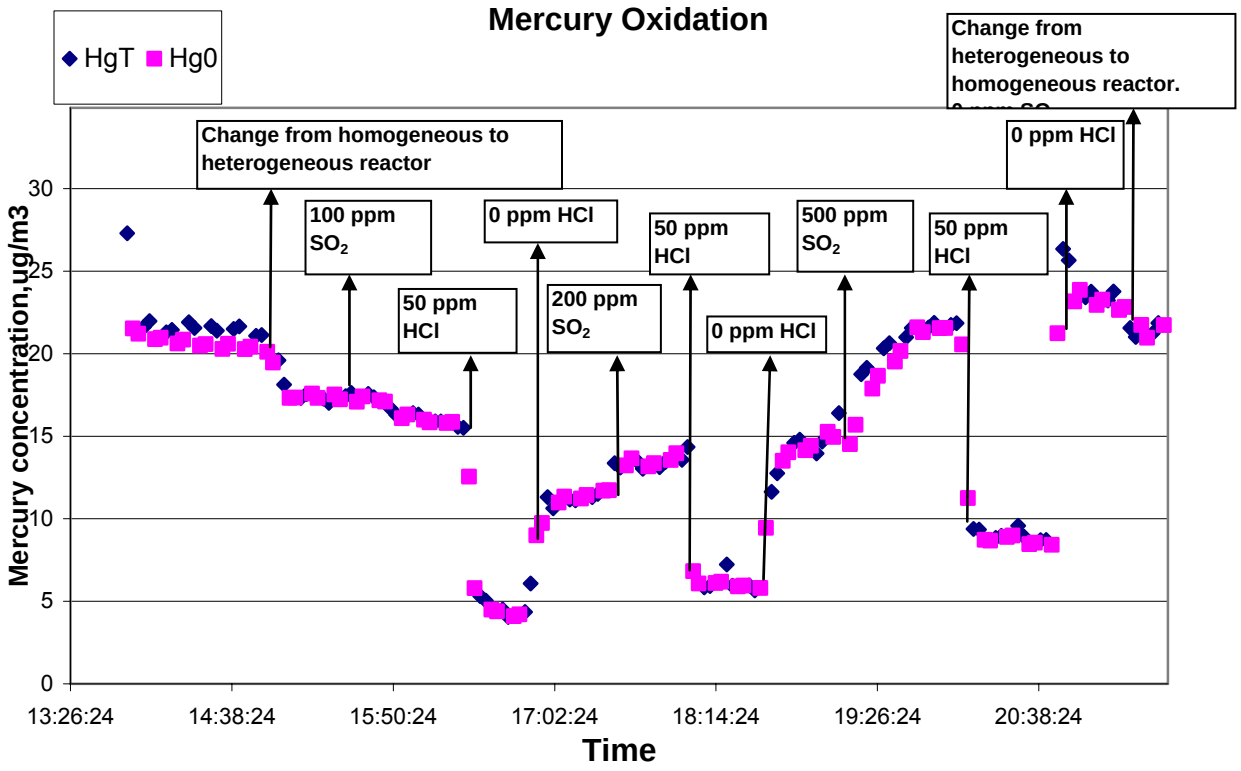

Figure 3 Elemental (Hg^0) and total (Hg^T) mercury concentrations at the exit of the carbon bed as a function of time (hours) at a temperature of 150°C at SO_2 concentrations of 100, 200, 500 ppm and a chlorine concentration of 50 ppm (as HCl equivalent).

The effect of bromine on mercury adsorption was also studied. As shown in Figure 4, the bromine causes an increase on mercury adsorption by the carbon and this increase is not affected significantly by either chlorine when added at 50 ppm (as HCl equivalent) or by SO_2 when added at 500 ppm, according to the results in Figure 5. Bromine as a promoter of adsorption or oxidation on activated carbon is less sensitive to SO_2 than chlorine.

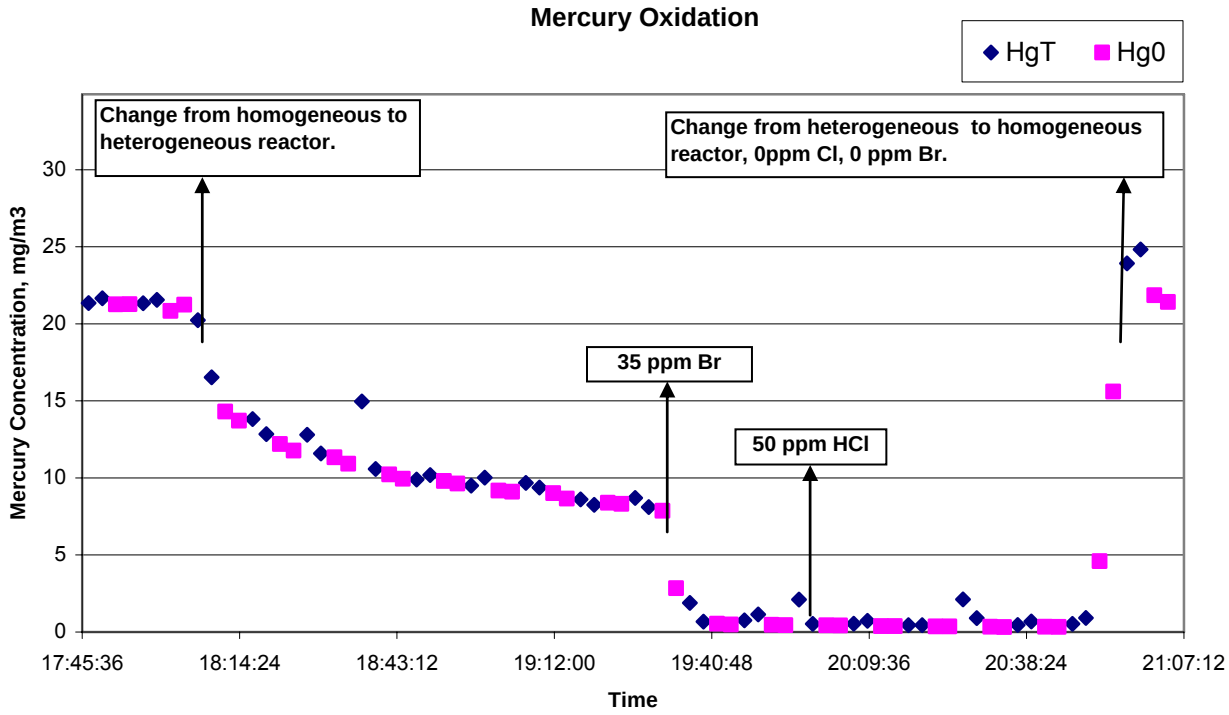

Figure 4 Elemental (Hg^0) and total (Hg^T) mercury concentrations at the exit of the carbon bed as a function of time (hours) at a temperature of 150^{o}C at a bromine concentration of 35 ppm (as HBr equivalent) and a chlorine concentration of 50 ppm (as HCl equivalent).

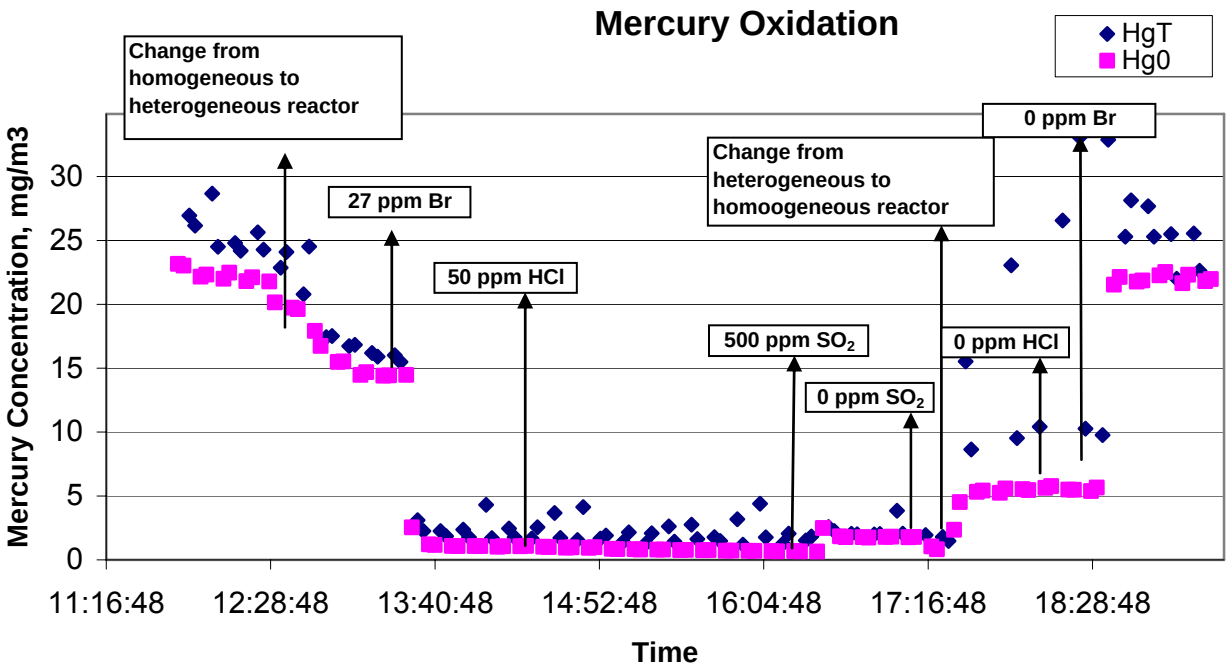

Figure 5 Elemental (Hg^0) and total (Hg^T) mercury concentrations at the exit of the carbon bed as a function of time (hours) at a temperature of 150°C at a bromine concentration of 27 ppm (as HBr equivalent) , chlorine concentration of 50 ppm (as HCl equivalent) and SO_2 concentration of 500 ppm.

A preliminary test was performed to study the effect of NO_2 on mercury adsorption and oxidation by the coconut-shell carbon. Because NO_2 is such a strong oxidant, this initial test was made by injecting the NO_2 through one of the bottom ports of the homogeneous reactor, instead of through the burner as is usual. Two NO_2 concentrations, 5 and 20 ppm, were used. For the homogeneous part of the test, no change was observed in elemental and total mercury concentrations at the exit of the homogeneous reactor at either concentration. Similar results were obtained with the heterogeneous reactor. Both sets of data are shown in Figure 6. Additional tests are planned to confirm these preliminary findings.

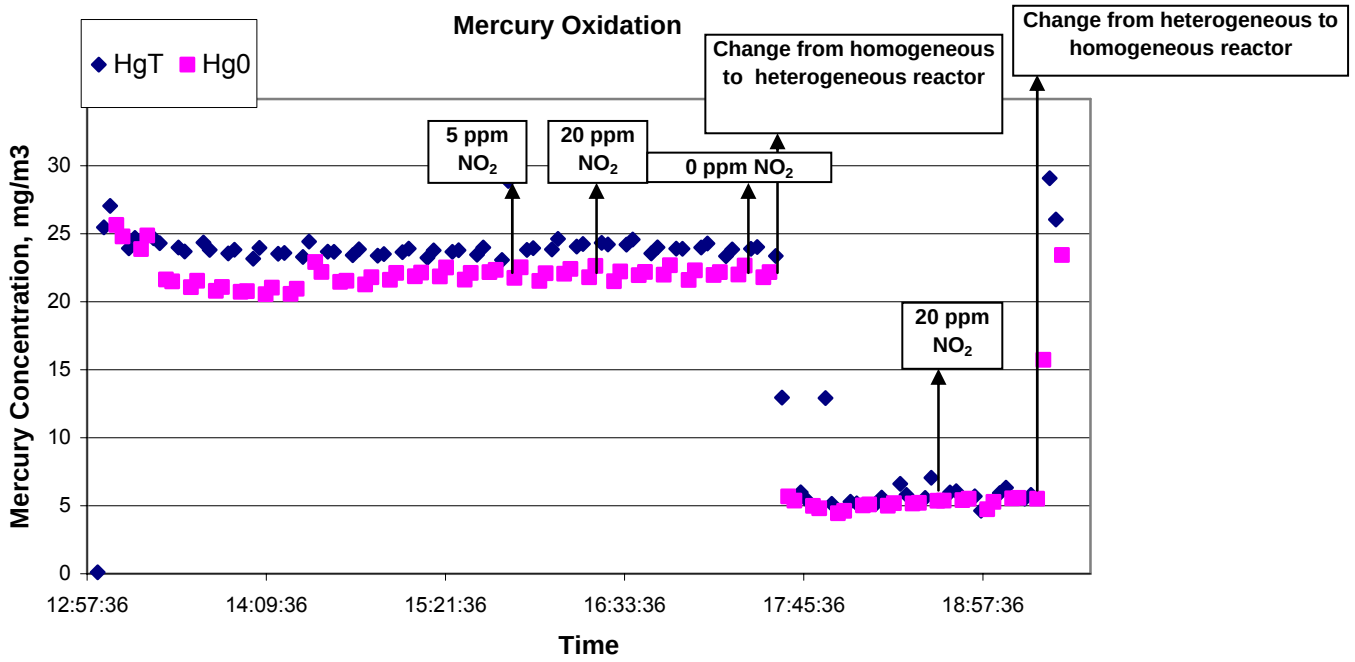

Figure 6 Elemental (Hg^0) and total (Hg^T) mercury concentrations at the exit of the carbon bed as a function of time (hours) at a temperature of 150°C at NO_2 concentrations of 5 and 20 ppm.

Heterogeneous Model

Packed bed

Following the Langmuir theory, the net rate of mercury adsorption on the activated carbon particle for species i can be written as the difference between the local adsorption rate and desorption rate:

$$\frac{dW_i}{dt} = k_{1i}\left(W_{\max,i} - \sum_{i=1}^{n} W_i\right)C_i - k_{2i}W_i \qquad (1)$$

where

$W_{max,i}$: Asymptotic adsorbate concentration (g Hg / g carbon).
K_{1i}: Kinetic constant of the adsorption reaction (m^3 / g min).
K_{2i}: Kinetic constant of the desorption (min^{-1}).
C_i: Gas phase concentration of component A (g / m^3).
W_i: Solid phase concentration of component A (g Hg / g carbon).
n: Number of species in the flue gas.
t: Time (min).

The mass balance in the gas phase in axial coordinates for species i is:

$$V\frac{dC_i}{dz}-\rho\frac{dW_i}{dt}=\varepsilon\frac{dC_i}{dt} \qquad (2)$$

where

ρ: Bulk density of the carbon (g carbon/m^3).
ε: Porosity of the bed (void fraction).

and

$$\varepsilon=\frac{Void\ volume}{Bed\ volume}=\frac{Bed\ volume-Carbon\ volume}{Bed\ volume} \qquad (3)$$

$$Bed\ volume=\frac{\pi}{4}D^2L-\frac{m_q}{\rho_q} \qquad (4)$$

$$Carbon\ volume=\frac{g_c}{\rho} \qquad (5)$$

where

D: Diameter of the packed bed (m).
m_q: Mass of quartz beads in the packed bed (g).
ρ_q: Quartz density (g/m^3).
L: Length of the packed bed (m).
A: Cross- Sectional area of the bed (m^2).
ΔZ : Distance between nodes (m).
V: Superficial velocity (m/min).

Equations (1) and (2), one for the gas phase and the other one for the solid phase, for all species, were discretized using forward discretization for the time derivatives and upwind discretization for the spatial derivatives .The discretized equations were solved using MATLAB.

As a first approach, breakthrough data and Langmuir constants from Karatza et al. [3] for $HgCl_2$ were used to determine the accuracy of the model and method of solution. Karatza's bed consisted of 50 mg of fly ash mixed with 3 grams of inert glass beads. The thickness of the bed was 2.5 mm, and an additional 57.5 mm of glass beads were provided upstream of the bed in order to distribute the gas flow over the entire cross section.

Using values of W_{max} = 0.00103 (g/g), k_1 =22.2 m^3/g min, k_2 = 0.033 min^{-1} from Karatza et al. [3] a fair fitting of the experimental data is observed, as shown in

Figure 7, where two sets of experimental data taken at 150°C were used. In A an initial $HgCl_2$ concentration of 2.8 mg/m^3 was used while in B this concentration was 10 mg/m^3.

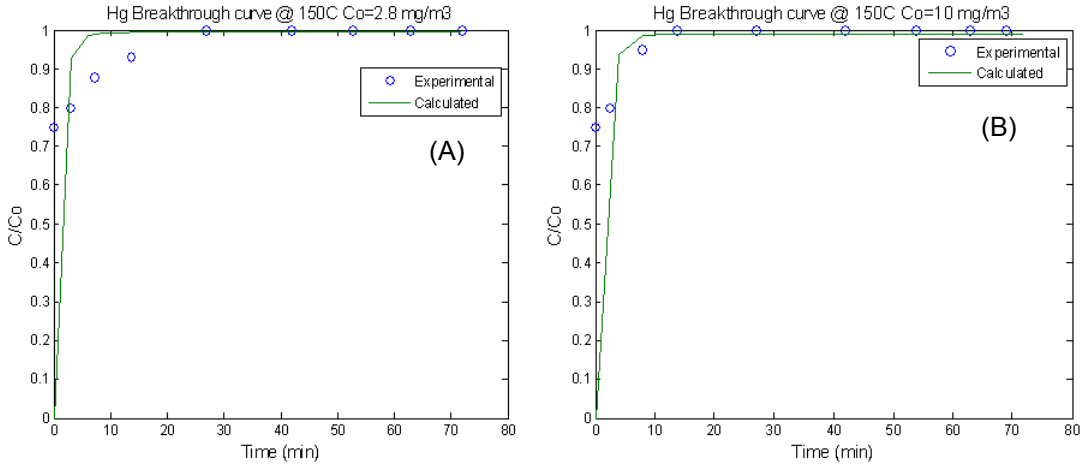

Figure 7 Breakthrough curves for fly ash with a bed temperature of 150°C. (A) Initial mercury concentration, C_o=2.8 mg/m3, (B) C_o=10mg/m^3. Experimental data from Karatza et al. [3]. Calculated values obtained with the heterogeneous model.

Figure 7 illustrates the accuracy of the heterogeneous model and method of solution for the two model equations. Other sources of experimental data [4] were used with the objective of finding the model constants for mercury and some of the other species in the flue gas (HCl, SO_2, and NO_2).

Miller et al. [4] used a quartz filter loaded with 150.5 mg of a carbon based sorbent and exposed it to a simulated flue gas. The temperature was kept at 225°F (107°C) and a Semtech 2000 mercury analyzer was used to continuously measure the elemental mercury at the outlet. A $SnCl_2$ reduction cell was used prior to the analyzer to convert all forms of mercury for analysis. With the reduction cell in place, the analyzer measured total mercury, but without the reduction cell only Hg^0 was measured. The baseline flue gas composition was O_2 6%, CO_2 12%, H_2O 8%, N_2 balance. Experimental results obtained by Miller et al. are shown in Figure 8 as well as the model results. A rough fitting of experimental and calculated data is observed using the parameter values from Table 1. As seen in this table, parameters can vary by orders of magnitude (e.g., maximum carbon uptake), particularly as the flue gas composition changes.

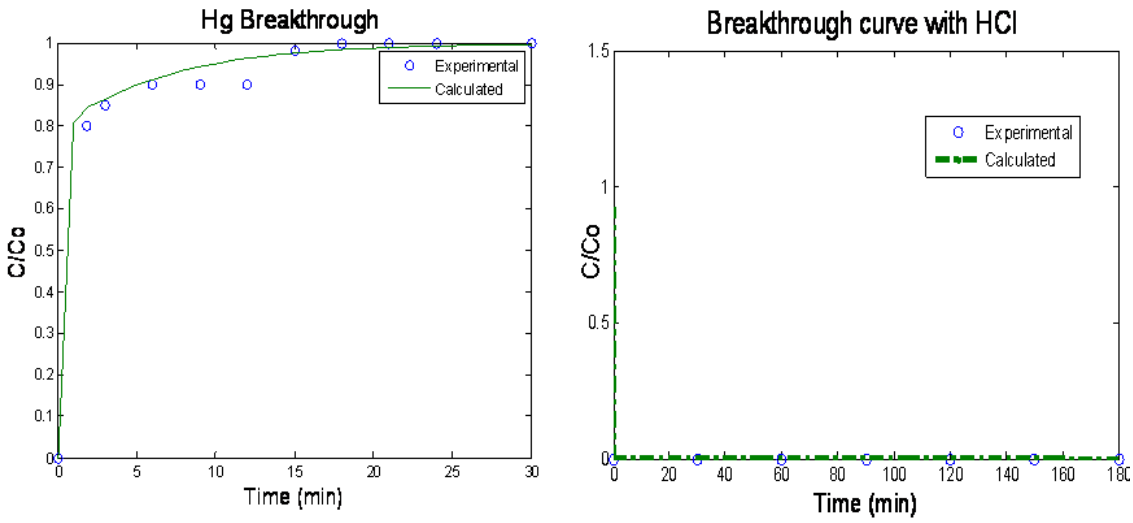

Figure 8 Breakthrough curves lignite activated carbon with a bed temperature of 107°C. (A) Mercury and baseline gases, (B) Mercury, 50 ppm HCl and baseline gases. Experimental data o from Miller et al. [4] Calculated data obtained with the heterogeneous model.

Table 1 Calculated heterogeneous model parameters for Miller et al. [4] experimental data.

Flue gas Composition	K_{1i} (m^3/g min)	K_{2i} (min^{-1})	W_{maxi} (g Hg/g Carbon)
Mercury and Baseline gases (i=1)	5.9212	0.1476	0.009105
Mercury, 50 ppm HCl and baseline gases (i=2)	3.05	268.992	0.091

Miller et al. [4] also used 0.15 g of lignite activated carbon to make a bed of 6.35 cm ID and 0.00947 cm depth at 225°F (107°C) and exposed it to a different flue gas compositions. The baseline composition was O_2 6%, CO_2 12%, H_2O 8%. In this case the fitting of the data is shown in Figure 9, using the model parameters shown in Table 2.

Table 2 Calculated heterogeneous model parameters for Miller et al. [4] experimental data.

Flue gas Composition	K_{1i} (m^3/g min)	K_{2i} (min^{-1})	W_{maxi} (g Hg/g Carbon)
Mercury and Baseline gases (i=1)	5.9212	0.1476	0.009105
Mercury, 1600 ppm SO_2 and baseline gases (i=2)	0.02870	0.5874	0.00751
Mercury, 20 ppm NO_2 and baseline gases (i=3)	2.8720	587.4	0.0751

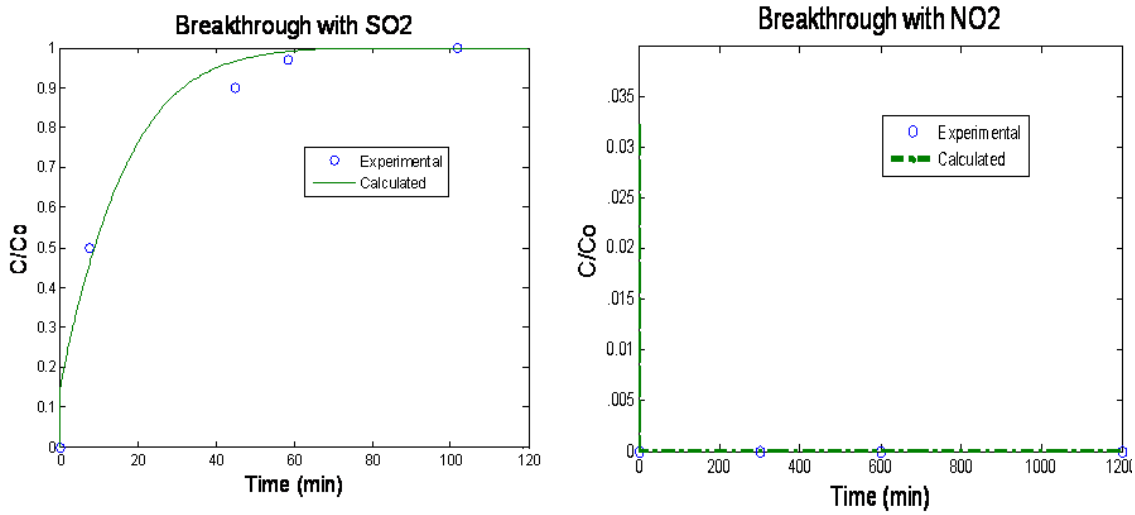

Figure 9 Breakthrough curves lignite activated carbon with a bed temperature of 107°C. (A) Mercury, 1600 ppm SO_2 and baseline gases, (B) Mercury, 20 ppm NO_2 and baseline gases. Experimental data o from Miller et al [4], Calculated data obtained with the heterogeneous model.

Single particle model for in flight sorbent capture of mercury

A mercury mass balance on the gas phase can be constructed using a conventional balance on an entire spherical sorbent particle or on adjacent, concentric shells within the particle where,

$$\text{Accumulation} = \text{Flux In} - \text{Flux Out} - \text{Adsorbed} \qquad (6)$$

The sign convention of the model treats flux into the particle as "positive" and flux out of the particle as "negative." Equation 6 may be expressed in differential form as,

$$\frac{\partial C_{cv}}{\partial t} V_{cv,i} \epsilon_P = J_{in} A_{in} - J_{out} A_{out} - R_{ads} V_{cv} \tag{7}$$

where

$C_{cv,i}$: Gas phase mercury concentration in the void space of the particle at the node i (g Hg/m^3)
$V_{cv,i}$: Volume of the shell at the node i (m^3).
ε_p: Porosity of the particle (m^3 void/ m^3 particle).
J_{in}: Gas phase mercury flux through the “in” side shell of the control volume (g Hg/ m^2 s).
A_{in}: Surface area of the particle side shell of the control volume (m^2).
J_{out}: Gas phase mercury flux through the “out” side shell of the control volume (g Hg/m^2 s).
A_{out}: Surface area of the bulk side shell of the control volume (m^2).
R_{ads}: Rate term for solid phase uptake of mercury (g Hg/s m^3).

The flux terms in Equation 7 follow Fick's law,

$$J = -D_{eff} \frac{\partial C}{\partial r} \tag{8}$$

where

Deff: Effective diffusivity of gaseous, elemental mercury inside the particle (m^2/s).
r: Radial distance from the center of the particle (m).

Once designated spatially, they may be discretized as,

$$J_{in} = -D_{eff} \frac{C_{center} - C_{in}}{\Delta r} \tag{9}$$

$$J_{out} = D_{eff} \frac{C_{center} - C_{out}}{\Delta r} \tag{10}$$

where:

C_{center}: Gas phase mercury concentration at the node inside of the control (g Hg/m^3).
C_{in}: Gas phase mercury concentration at the “in” side shell of the control Volume (g Hg/m^3).
C_{out}: Gas phase mercury concentration at the “out” side shell of the control

volume (g Hg/m^3).

Δr: Radial distance between adjacent shells (m).

and substituted back into Equation 7 to form Equation 11,

$$\frac{\partial C_{cv}}{\partial t} V_{cv,i} \epsilon_P = -D_{eff} \left(\frac{C_{center} - C_{in}}{\Delta r} \right) A_{in} - D_{eff} \left(\frac{C_{center} - C_{out}}{\Delta r} \right) A_{out} - R_{ads} V_{cv} \qquad (11)$$

The spatial orientation of the concentration terms may be standardized with respect to index i.

$$C_{center} = C_i \qquad (12)$$

$$C_{in} = C_{i-1} \qquad (13)$$

$$C_{out} = C_{i+1} \qquad (14)$$

Additionally, the volume and area terms may also be spatially specified with index value i. Once the terms are given a spatial index, they may be regrouped and equation 11 simplifies to,

$$\frac{dC_{cv,i}}{dt} = \frac{D_{eff}}{V_{cv,i} \epsilon_P \Delta r} \left(C_{i-1} A_{i-1} - C_i (A_{i-1} + A_i) + C_{i+1} A_i \right) - \frac{R_{ads}}{\epsilon_P} \qquad (15)$$

Graphically, the concentration, area, and volume terms from Equation 15 may be represented as shown in Figure 10. The adjacent shells in the mass balance are organized by index value, i, into nz nodes. At i=nz, the nodes terminate at the particle's surface where the subscript R maybe used interchangeably with nz. The organization of the general mass balance terms is shown in Figure 11.

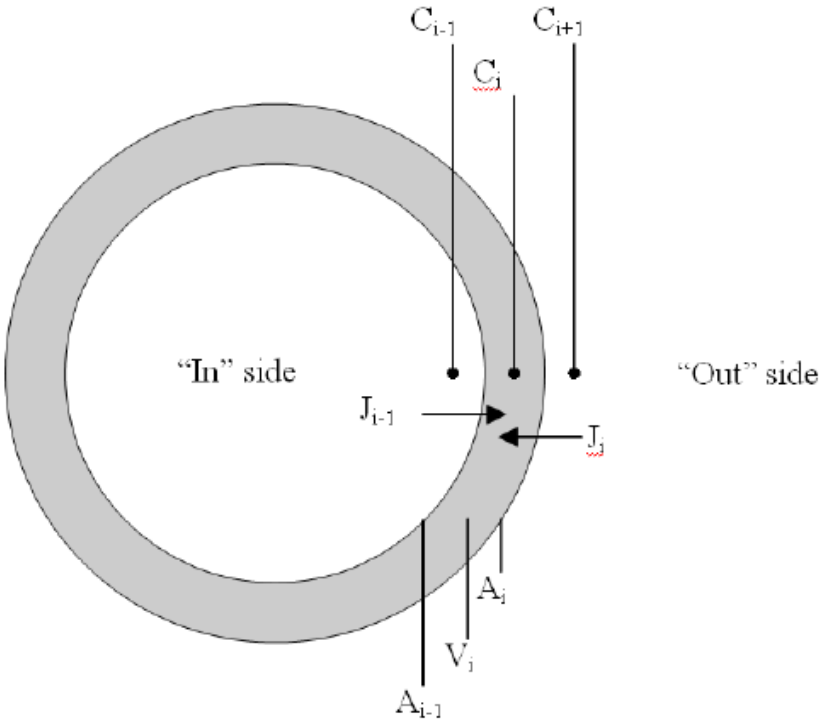

Figure 10 The basic mass balance scheme used in a shell inside a uniform, spherical sorbent particle.

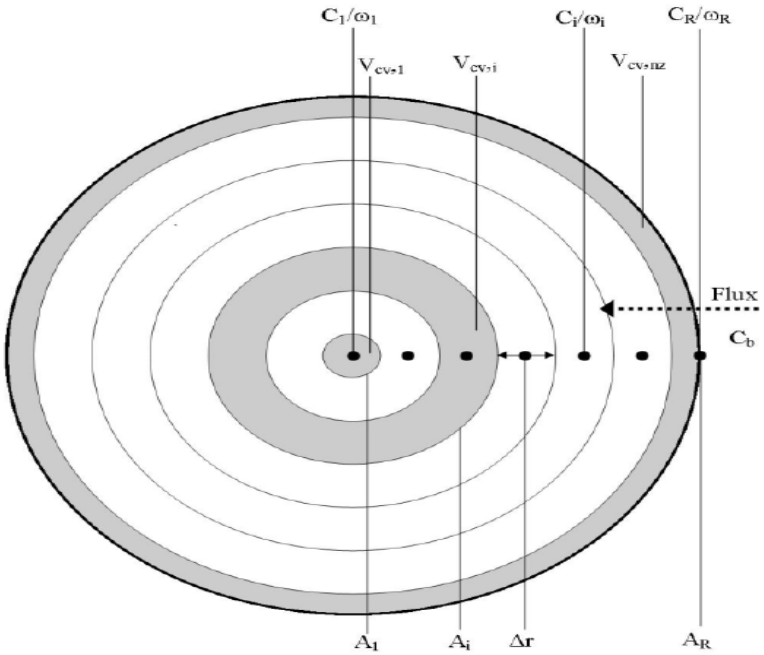

Figure 11 The organization of the discretization scheme used in the model.

Rate Models

The effective diffusion coefficient from Equations 9 and 10 may be calculated by combining the Knudsen and binary diffusion coefficients:

$$D_{eff} = \frac{\tau_P^{-1}}{1/D_{ab} + 1/D_{kn}} \tag{16}$$

where

τ: Sorbent particle tortuosity
D_{ab}: Binary diffusion constant between gaseous mercury and air (m^2/s).
D_{kn}: Knudsen diffusion coefficient (m^2/s).

The binary diffusion coefficient may be computed using the classic Chapman-Enskog equation and the appropriate constants [5,6]. The Knudsen diffusion coefficient and tortuosity may be computed using Equations 17 and 18.

$$D_{kn} = \frac{97}{2} d_{pore} \left(\frac{T}{MW_{Hg}}\right)^{0.5} \tag{17}$$

$$\tau_P = \epsilon_P^{-1.5} \tag{18}$$

where

d_{pore}: Average pore diameter of the sorbent particle (m).
T; Reactor temperature (K).
MW_{Hg}: Molecular weight of mercury (g Hg/mole).

The form of R_{ads} in the Equation 15 is dependent upon the apparent density of the sorbent particle, ρ_p, and a solid phase rate model. In this work, three different rate models are employed. The first and simplest uses a difference between adsorption and desorption,

$$\frac{\partial \omega_i}{\partial t} = k_1(\omega_{max} - \omega_i)C_{cv,i} - k_2\omega_i \tag{19}$$

where

ω_i: Solid phase, elemental mercury concentration at node i (g Hg/g carbon).
ω_{max}: Maximum elemental mercury uptake capacity of the sorbent (g Hg/ g carbon).
k_1: Adsorption constant (m^2/ g Hg s).
k_2: Desorption constant (1/s).

If equilibrium is assumed at the surface of the particle,

$$k_2\omega_i = k_1(\omega_{max} - \omega_i)C_{cv,i} \tag{20}$$

$$k_2\omega_i = k_1\omega_{max}C - k_1\omega_i C_{cv,i} \tag{21}$$

$$(k_2 + k_1 C_{cv,i})\omega_i = k_1\omega_{max}C_{cv,i} \tag{22}$$

$$\omega_i = \left(\frac{k_1\omega_{max}C_{cv,i}}{k_2 + k_1 C_{cv,i}}\right) \tag{23}$$

$$\omega_i = \left(\frac{K_{lang}\omega_{max}C_{cv,i}}{1 + K_{lang}C_{cv,i}}\right), \quad K_{lang} = \frac{k_1}{k_2} \tag{24}$$

where

K_{lang}: Sorption constant for Langmuir Isotherm (m^3/g Hg).

Equation 24 is the adsorption component of the second rate model and is known as the Langmuir isotherm. Finally a Freundlich isotherm may also be used in the rate model,

$$\omega_i = \frac{C_{cv,i}^{1/n}}{K_{fr}} \tag{25}$$

where

K_{fr}: Sorption constant for Freundlich isotherm.

Both the Langmuir and Freundlich models must be differentiated with respect to time before they can be used in the general mass balance in equation.

The boundaries of the shell balance require the initial conditions,

$$@t = 0, \quad C_{cv,i} = 0 \tag{26}$$

$$\omega_i = 0 \tag{27}$$

$$C_b = C_{bo} \tag{28}$$

where

C_b; Bulk, gas phase mercury concentration (g Hg/m^3).
C_{bo}: Inlet mercury concentration (g Hg/m^3).

The flux boundary condition,

$$@r = 0, \frac{\partial C_{cv,i}}{\partial r} = 0 \tag{29}$$

is also necessary in the solution of the shell balance. Mercury flux through the particle surface is equal to the amount lost from the bulk phase,

$$-D_{eff}\frac{\partial C_R}{\partial r} = k_{mt}(C_R - C_b) \tag{30}$$

where

C_R: Gas phase mercury concentration at particle surface (g Hg/m^3).
k_{mt}: External mass transfer coefficient (m/s).

When multiplied by the available external particle surface area, Ω, this quantity is equal to the change in bulk mercury concentration with respect to time as shown in Equation 31.

$$\frac{\partial C_b}{\partial t} = \Omega k_{mt}(C_R - C_b) \tag{31}$$

The mass transfer coefficient may be computed given the assumption that the boundary layer is stationary. As a sorbent particle falls through a duct, its terminal velocity may be computed by balancing the gravitational forces with the buoyant and kinetic forces as discussed by Bird, Stewart, and Lightfoot [7]. The force balance may be solved for the terminal velocity term to yield Equation 32.

$$v_{terminal} = \frac{2R_P^2(\rho_{Pactual} - \rho_{gas})g}{9\mu} \tag{32}$$

where

R_p: Sorbent particle radius (m).
$\rho_{Pactual}$: Actual density of the sorbent particle (g carbon/m^3).
g: Acceleration due to gravity (m/s^2).
vterminal: Speed at which a sorbent particle of radius Rp travels due to gravity alone (m/s).

Given a range of particle diameters from 1 to 75 microns, a flue gas composition comparable to air, and a temperature of 150°C, the terminal velocities of particles in a full scale duct will range from 7.4×10^{-4} to 4.1 meters per second whereas the linear velocity of flu gas in a full-scale duct is usually on the order of 20+ meters per second[8]. By the standard correlation [9]

$$N_{sh} = (4.0 + \frac{1.21(v_{terminal} * 2R_P}{D_{ab}})^{2/3})^{1/2} \tag{33}$$

where

N_{sh}: Sherwood number.
D_{ab}: Binary diffusion constant between gaseous mercury and air (m^2/s).

The Sherwood number then varies from 2.0 to 3.2. Small sorbent particles will travel roughly the same speed as the flue gas while the larger particles will travel slightly faster. The question may be asked as to whether a momentum balance is necessary to model in-flight uptake. Scala et al. [10] found that assuming a stationary boundary layer resulted in no more than 10 % error into the results and for that reason a similar assumption is made in this model.

The mass transfer coefficient is defined as,

$$k_{mt} = \frac{ShD_{ab}}{2R_P} \tag{34}$$

On account of the boundary condition in Equation 29, the "inner flux" term on the mass balance at the centermost node of the particle is zero. Therefore, Equation 15 when applied at that node is,

$$\frac{dC_{cv,1}}{dt} V_{cv,1} \epsilon_P = \frac{D_{eff} A_r}{\Delta r} \left(C_2 - C_1 \right) - R_{ads} V_{cv,1} \tag{35}$$

At the particle surface, the "outer" flux term must be expressed via Equation 15 as the index nz+1 does not exist on the sorbent particle.

In the mass balance, adsorption may also be assumed to take place only at the particle surface. In such a case, the governing equations are just as they were before only all of the "inner" flux terms are zero, and the balance on the particle surface is slightly simpler:

$$\frac{dC_R}{dt} = \frac{k_{mt}}{V_{cv,nz}\epsilon_P}(C_{Bulk} - C_R)A_R - \frac{R_{ads}}{\epsilon_P} \quad (36)$$

The balance for the bulk mercury concentration change is the same as Equation 31.

Model Solution

Equation 15 can be discretized into a series of adjacent shells and combined with Equations 31 and 36 to form a complete mass balance on the system. Before the equations can be solved, however, the user must specify a number of parameters. In each of the three R_{ads} models, a set of constants is required - ω_{max}, k_1, and k_2 for the standard adsorption/desorption model, ω_{max} and K for the Langmuir isotherm model, and n and K_{fr} for the Freundlich isotherm model. These parameters are commonly extracted from a packed bed isotherm [11]. Finally, ρ_P and the number of nodes to be used inside the particle must be specified.

The model calculates mercury uptake with respect to time, porosity, feed rate, average particle pore size, and particle radius. It can also calculate solid and gas phase concentrations inside the sorbent particle itself. Before running the code, parameter(s) to be varied and isotherm model(s) to be used must be specified. The model uses the MATLAB function "ode23s," a stiff ordinary differential equation solver, to obtain solutions.

The results from the rate law and Langmuir isotherm models can be compared directly as identical parameters may be applied to their governing equations. K_{lang} from the Langmuir isotherm is simply the quotient of k_1 and k_2 from the rate model. The parameters shown in the results for these two adsorption models are shown in Table 3.

Table 3 Constants used in Rate law and Langmuir isotherm adsorption models.

Parameter	Magnitude	Units
K	580.8	$\frac{m^3}{g}$
k_1	0.41	$\frac{m^3}{g \cdot s}$
k_2	7.06e-4	$\frac{1}{s}$
w_{max}	1000	$\frac{\mu g_{Hg}}{g_{carbon}}$
D_{ab}	2.55e-5	$\frac{m^2}{s}$
D_{kn}	7.0e-6	$\frac{m^2}{s}$
$F.R.$	10.0	$lb/MMacf\left(0.08\frac{g_{carbn}}{m^3}\right)$
R_P	14.5	μm
D_{pore}	3.0	nm
$t_{residence}$	2.0	s

Of the three R_{ads} models, the rate of adsorption/desorption model shows the lowest uptake. Under typical, full-scale conditions, mercury uptake under this model is virtually zero as can be seen in Figure 12. This negligible uptake is not

entirely unexpected as equilibrium, which is highly favorable for adsorption, is not fixed at the particle surface. Equilibrium at the particle surface allows for a solid phase concentration to exist as soon as gas phase mercury reaches the solid surface.

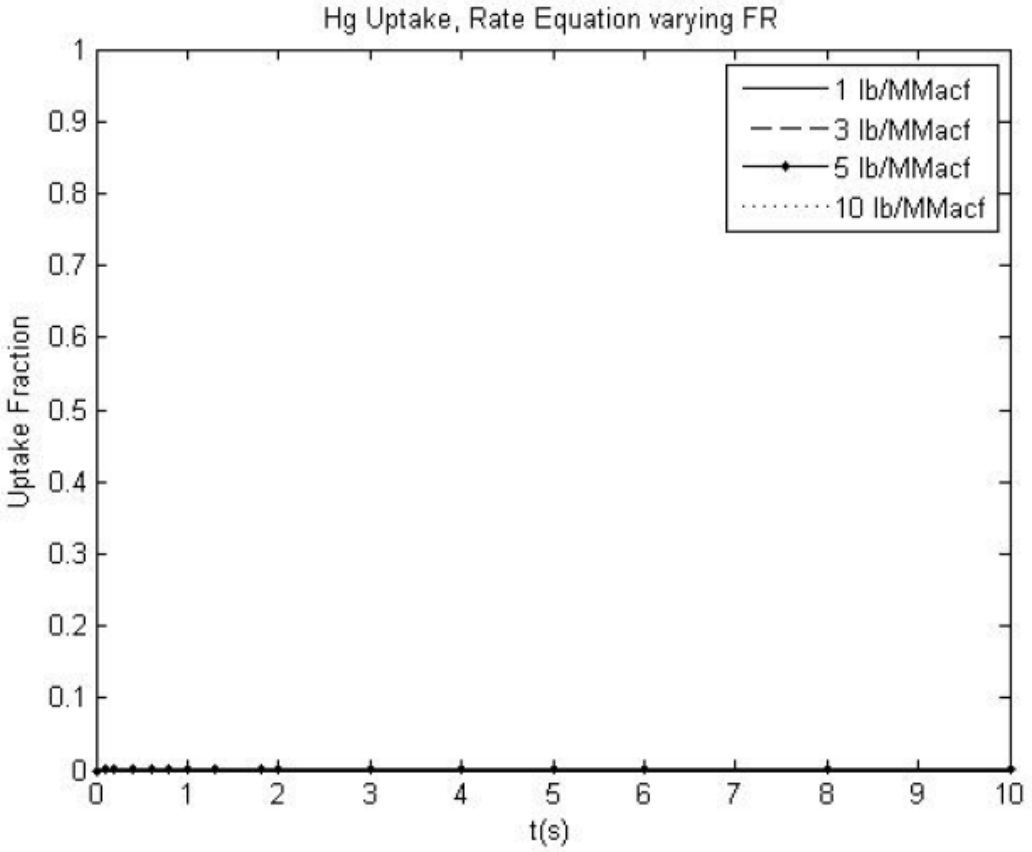

Figure 12 Mercury uptake normalized with inlet concentration over time using the rate model.

Figure 13 shows that even at a residence time as low as 2 seconds, gaseous mercury can enter the particle. Because the adsorption process takes more time to complete, the solid phase concentration is zero. In this figure and all subsequent figures containing solid phase concentrations, the intraparticle solid phase concentrations,_ωi, must be multiplied by feed rate, FR, and normalized with the inlet concentration, C_{bo}, in order to be compared directly to gas phase concentration.

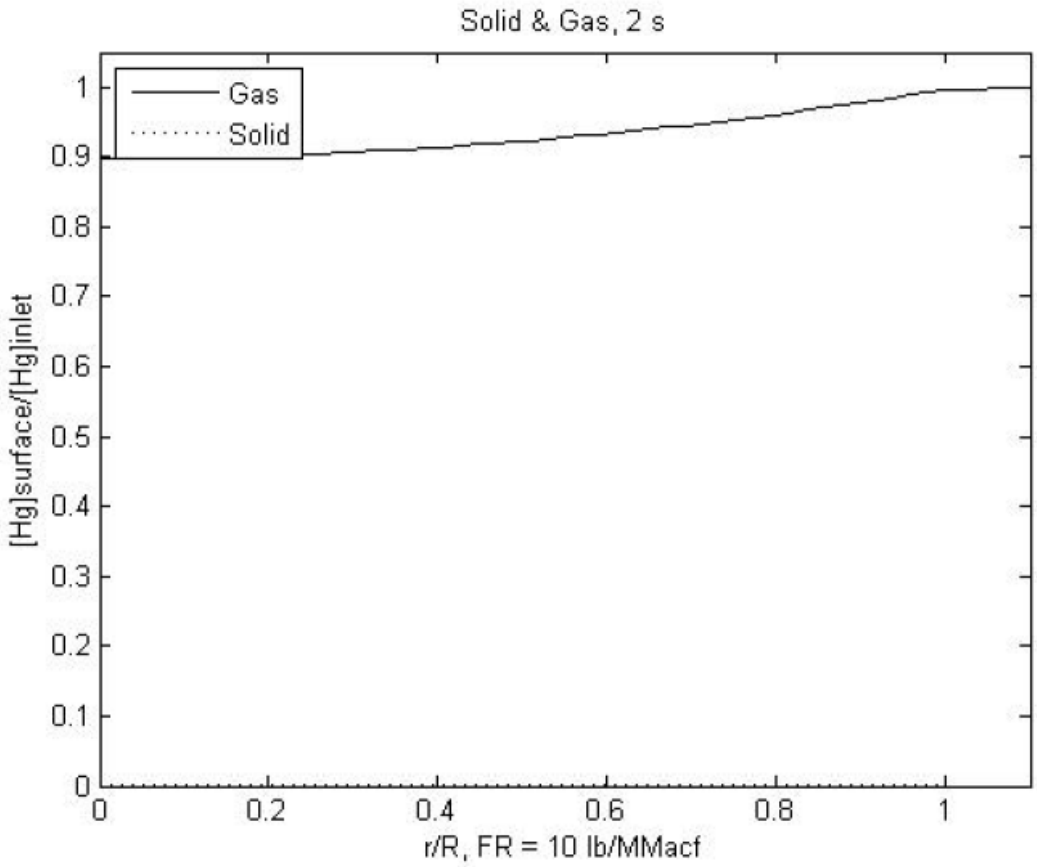

Figure 13 Mercury uptake normalized with inlet concentration in both the solid and gas phases using the rate model.

The results from the Langmuir isotherm adsorption model in Figure 14 show higher uptake levels than do the rate model results, but as stated for the rate model, this uptake is almost negligible under standard operating conditions. Similar results were obtained by Flora et al. [12] .

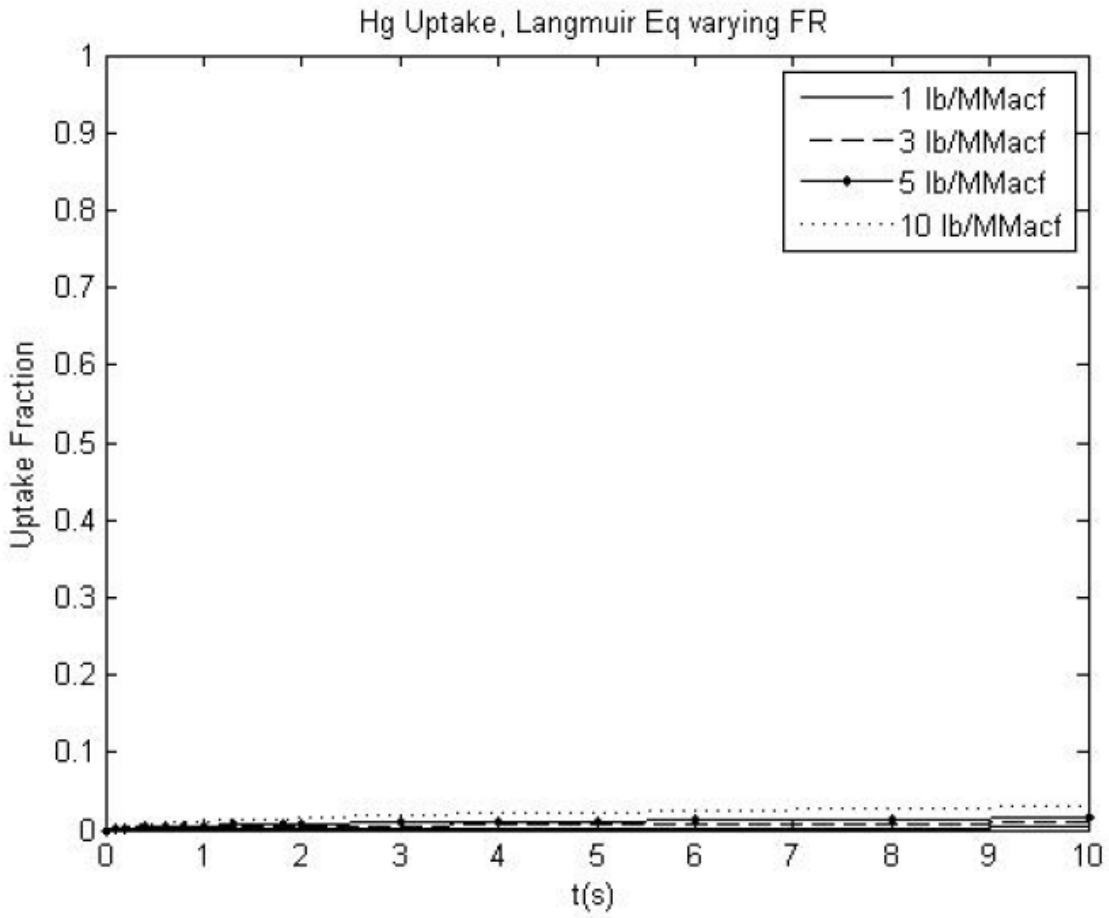

Figure 14 Mercury uptake normalized with inlet concentration over time using the Langmuir isotherm model.

At low residence times, some gas phase intraparticle concentration can be observed in the Langmuir model as shown in Figure 15.

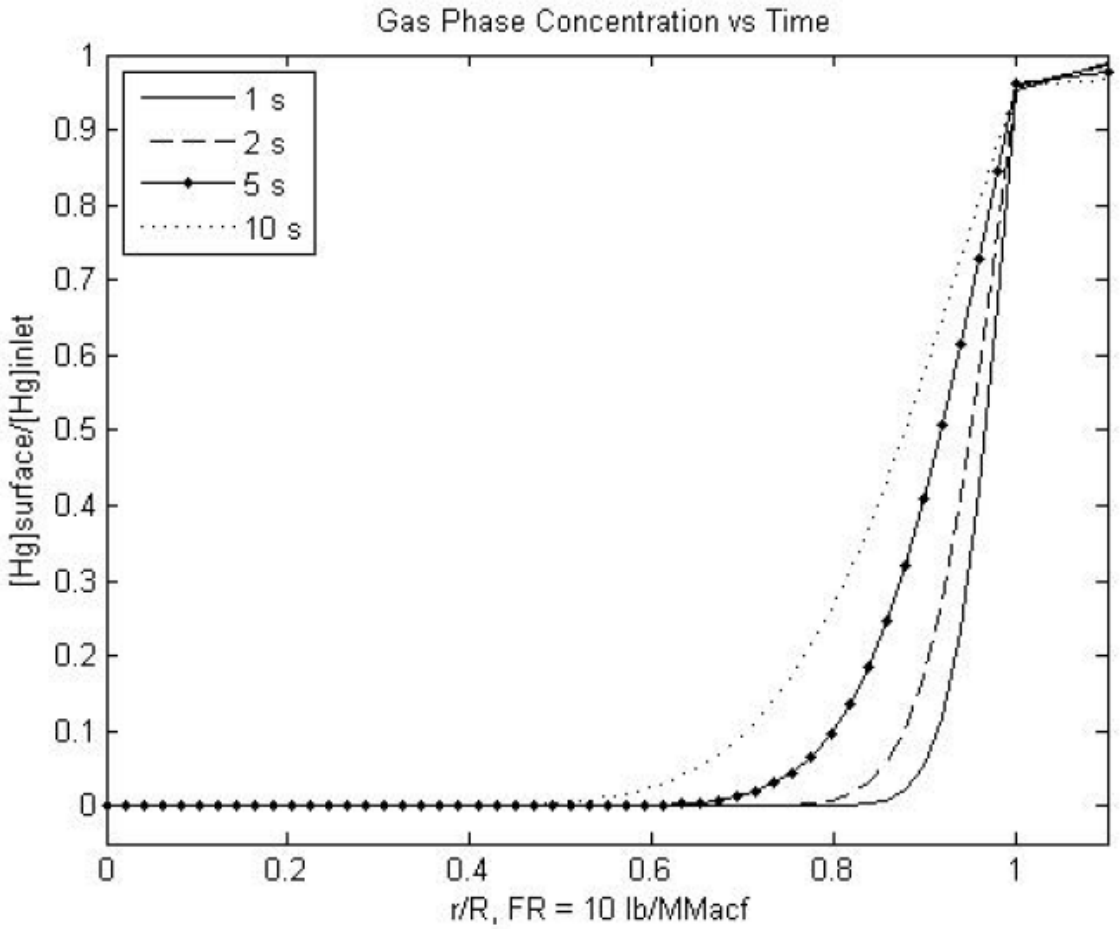

Figure 15 Mercury concentration normalized with inlet concentration inside the sorbent particle using Langmuir isotherm model.

The Freundlich isotherm parameters experimentally determined from a sorbent used in full-scale tests at Pleasant Prairie [8] are shown in Table 4. They are used in the Freundlich model results below along with reactor parameters similar to the ones used in the rate and Langmuir isotherm models.

Table 4 Constants used in Freundlich isotherm adsorption model.

Parameter	Magnitude	Units
K_{fr}	0.01490	$\frac{g_{carbon}}{m^3}$
n	1	
D_{ab}	2.55e-5	$\frac{m^2}{s}$
D_{kn}	7.0e-6	$\frac{m^2}{s}$
$F.R.$	10.0	$lb/MMacf\left(0.08\frac{g_{carbn}}{m^3}\right)$
R_P	14.5	μm
D_{pore}	3.0	nm
$t_{residence}$	2.0	s

Using the above magnitude for the necessary parameters, Figure 16 shows mercury uptake under the Freundlich isotherm adsorption model.

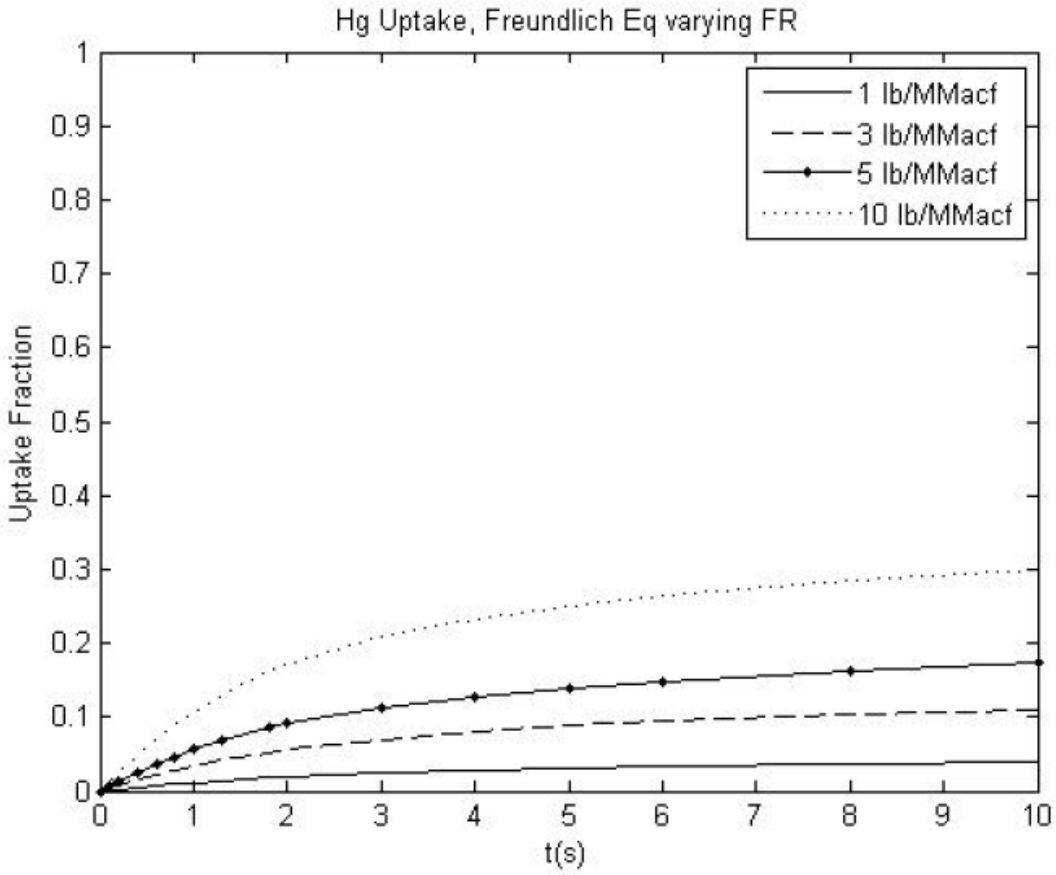

Figure 16 Mercury uptake normalized with inlet concentration over time using Freundlich isotherm model.

At normal residence times, a steep gas phase intraparticle concentration gradient can be observed in the Freundlich model as shown in Figure 17. This gradient is much steeper than that seen in the Langmuir adsorption model

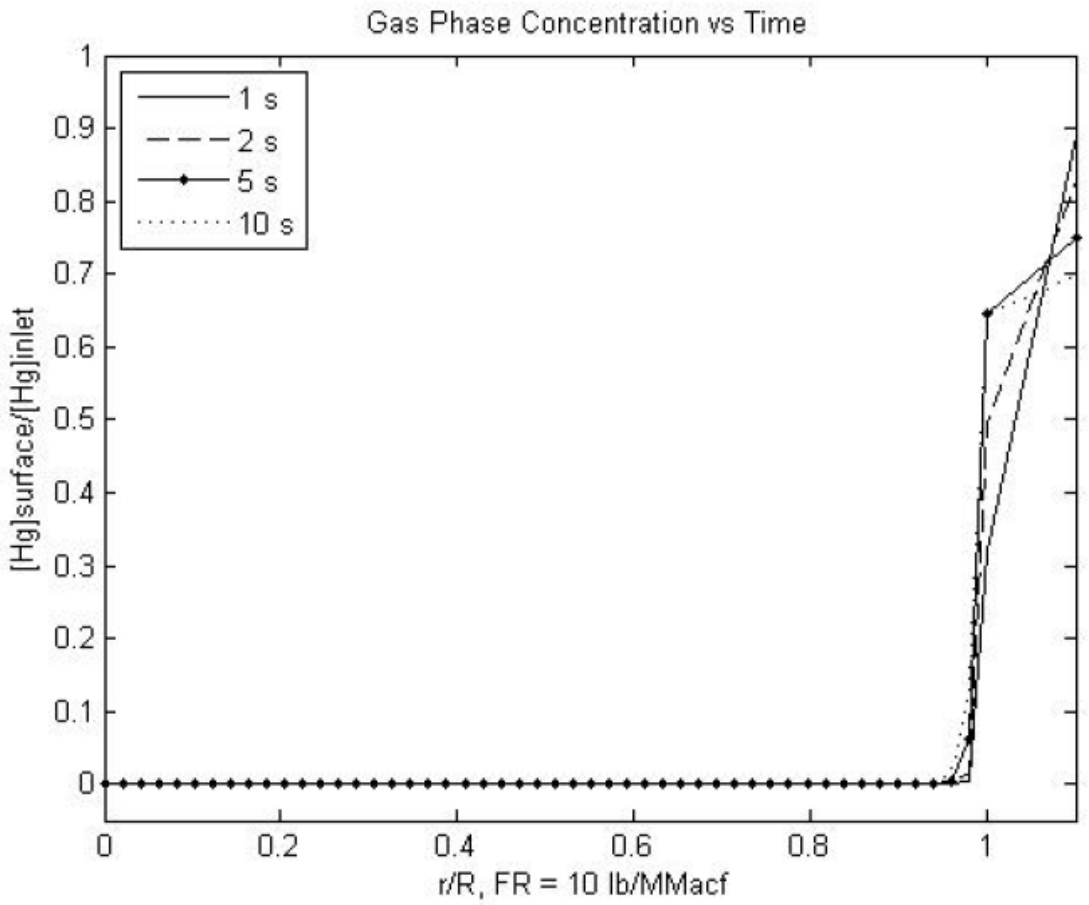

Figure 17 Mercury uptake normalized with inlet concentration over time using Freundlich isotherm model.

Effect of Individual Sorbent Properties

Theoretically, particle diameter greatly affects mercury uptake as shown in Figure 18. These results are similar to that seen in the other published work [11] . Mercury uptake is inversely proportional to particle diameter. As sorbent diameter decreases, more surface area is available for uptake. However, that diameter crosses a certain minimum values, external mass transfer becomes the primary resistive force to uptake.

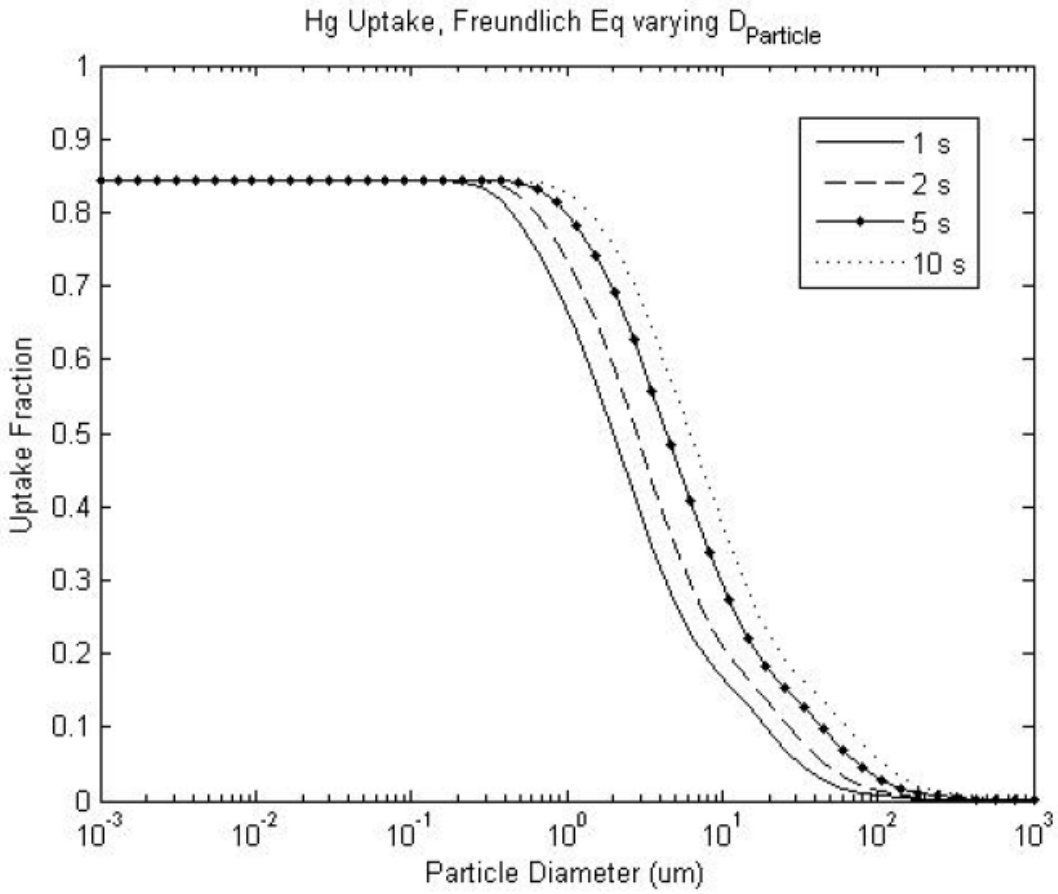

Figure 18 Mercury uptake normalized with inlet concentration over time using Freundlich isotherm model and varying particle diameter.

Multiple full scale reports have shown [8,13,14], however, that particle diameter does not affect mercury uptake as implied by models. This contradiction may likely be accounted for by poor dispersion of the particles as they are injected into the ducts. The Pollack report [14] commented on some attempts to verify this hypothesis by varying injection geometry to get different adsorption results. Adsorption under these altered conditions proved no different than the original test.

An alternate explanation lack of convergence between the model and full-scale data is that particle distributions are not properly addressed in models. With the exception the work by Meserole et al. [15], all published models assume a monodisperse size distributions. However, the sorbents used in full-scale settings have polydisperse size distributions. In order to capture this effect, sorbent particles in a model may be "binned" at any resolution desired. The "binned" conditions modeled in Figure 20 simulate the distribution reported by Cremer et al [8] in Figure 19.

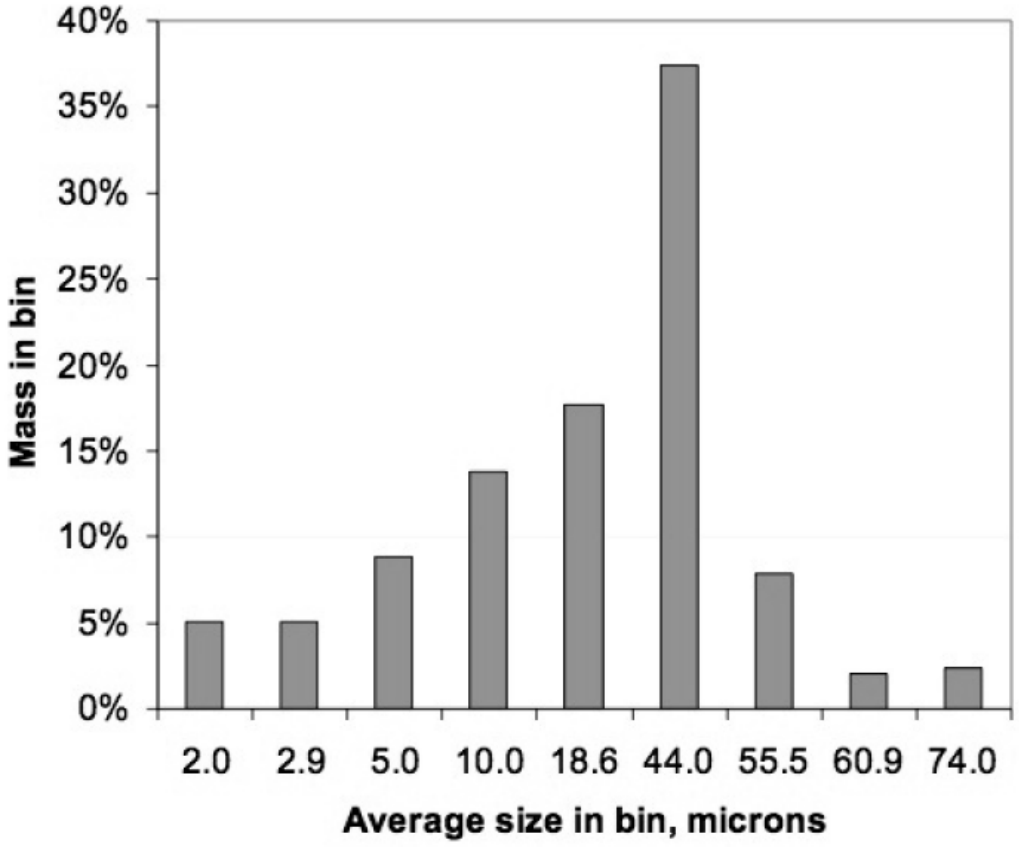

Figure 19 One example of how activated carbon particles may be distributed in "bin" form.

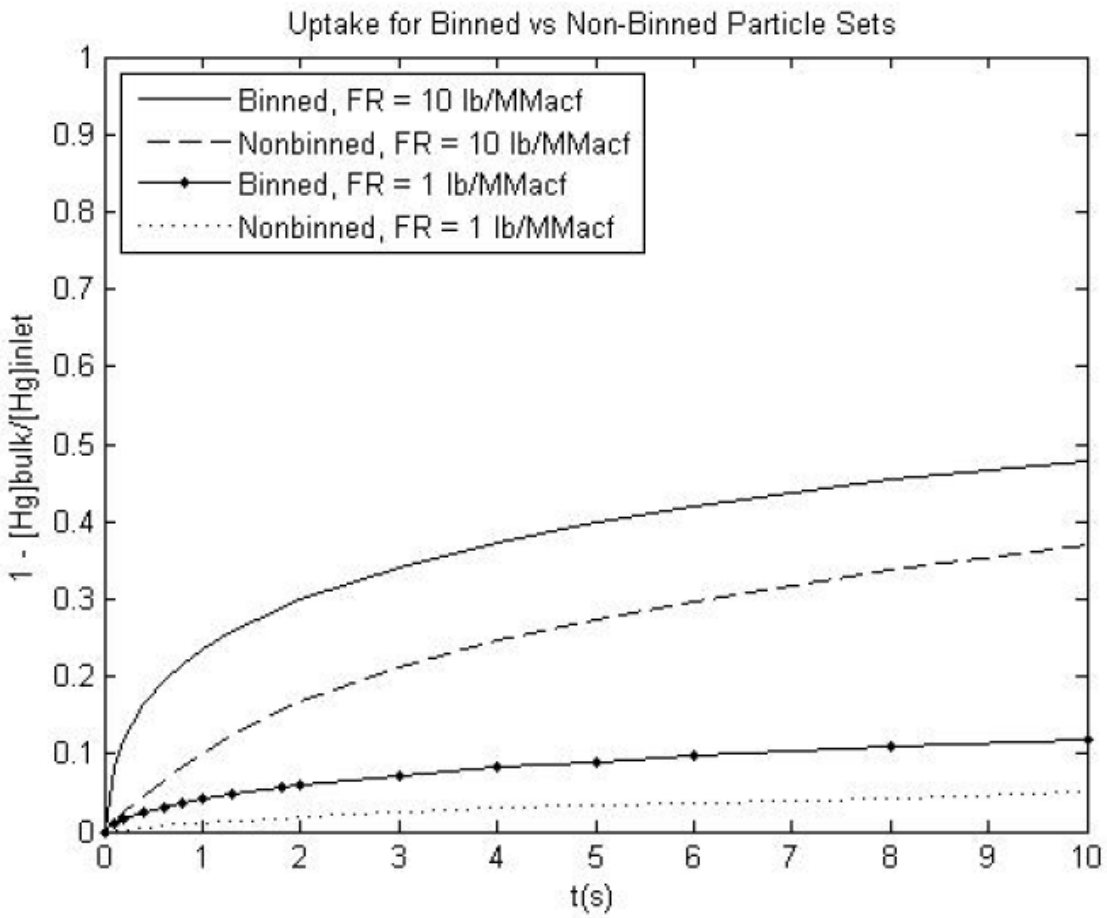

Figure 20 A comparison of uptake for “binned” and “nonbinned” particle sets for two different feed rates. “Binned” at size range from 2 μm to 75 μm and averaging 30 μm which is the size angle used in the “nonbinned” model.

Figure 21 shows a direct comparison of the 1 and 10 lb/MMacf lines from the "nonbinned" particles in Figure 20 and the "binned" particles previously described. The "binned" model show significantly more uptake than does the "nonbinned" model due to the presence of smaller than average particles that, per capita, have more surface area exposed directly to the bulk. The "nonbinned" particle set has an average diameter of 29 μm which is identical to the average diameter of the "binned" set.

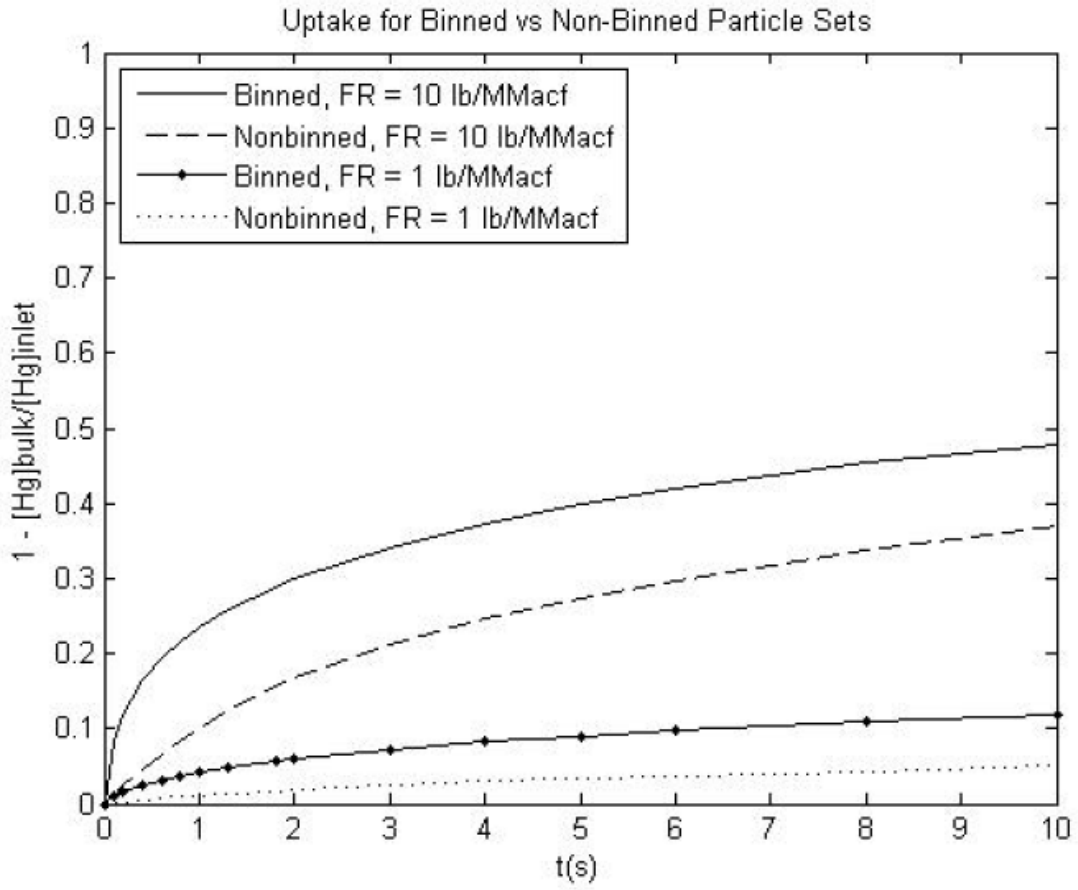

Figure 21 A comparison of uptake for "binned" and "nonbinned" particle sets for two different feed rates. "Binned" at size range from 2 μm to 75 μm and averaging 30 μm which is the size angle used in the "nonbinned" model.

These results show that the two systems with the same average particle diameter may have different adsorptive capacities depending on the actual distribution and the need for including particle size distribution in a model.

Nonlinearity of Feed Rate influence on uptake

Full scale data has shown that mercury uptake does not increase linearly with feed rate [8]. While this effect is observed in Figure 22, the cause is likely different. Most full scale data show that mercury uptake maximizes between 10 and 15 lb/MMacf. As shown in the figure, the model requires a great deal more sorbent before the maximum limit is reached. One possible case as discussed by the Pollack report [14] could be an actual change in adsorptive capacity due to lowering chlorine concentrations in the full-scale results. This was found in the packed bed study as well (see Table 1). Another possibility mentioned by the Pollack report is the hypothesis that the injection lances are not properly distributing the sorbent.

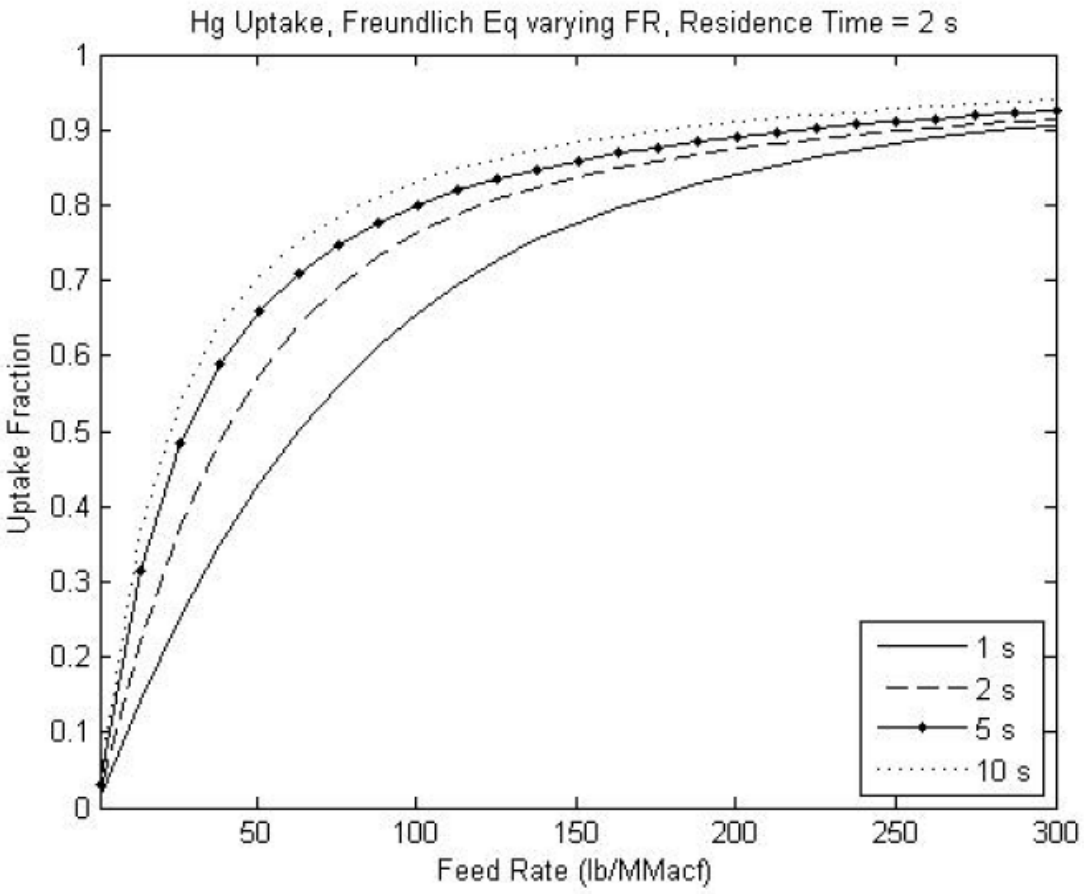

Figure 22 Mercury uptake normalized with inlet concentration over time using the Freundlich isotherm model and varying the feed rate (Rp=15 μm).

Consolidation of Adsorption Models

Calculations with actual sorbents, realistic reactor settings, and the Langmuir isotherm results in Figure 14 are significantly lower than what is shown in full-scale data [8,13]. In order to understand this inconsistency, several parameters must be investigated.

External mass transfer easily becomes a resistive force when particle size is large enough. By increasing D_{ab} by 4 orders of magnitude, external mass transfer can effectively be removed from the Langmuir model. The results are shown in Figure 23. Mercury uptake is still low overall, so external mass transfer is clearly not the limiting factor in adsorption.

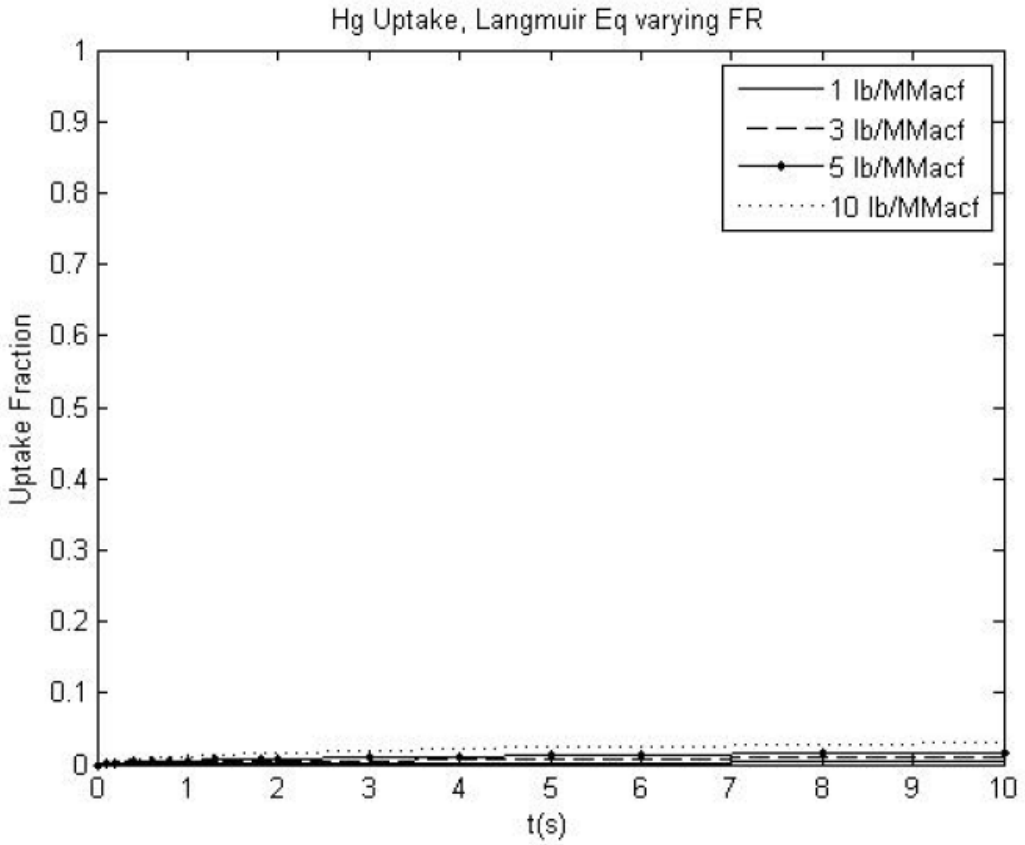

Figure 23 Mercury uptake normalized with inlet concentration over time using the Freundlich isotherm model and maximizing Dab to minimize resistance from external mass transfer (R_p=15μm).

Additionally, the Langmuir isotherm also takes around 100 seconds to reach its maximum value - much longer than any residence time in a full scale system. This observation is consistent with the results from the Langmuir model constructed by Flora et al. [12] who reported no more than 2% uptake in the entire entrained portion of a reactor using Darco-FGD carbon.

The uptake results from the Freundlich isotherm adsorption model shown in Figure 16 are higher than those in the other two models, but it is not immediately clear that the Freundlich isotherm model itself more closely simulates the adsorption of mercury onto activated carbon. Though the Freundlich and Langmuir isotherms have different forms, at standard flue gas concentrations and ω_{max} values seen in realistic settings, they are mathematically similar.

As $K_{lang}C$ gets smaller, the Langmuir isotherm, Equation 24, simplifies to

$$\omega_i = K_{lang}\omega_{max}C_{cv,i} \qquad \text{(Eq. 37)} \quad (37)$$

If n from the Freundlich isotherm is assumed to be 1 and the Freundlich sorption constant, K_{fr}, is defined as,

$$K_{fr} = \frac{1}{K\omega_{max}} \tag{38}$$

The Freundlich isotherm takes the form,

$$\begin{aligned} \omega_i &= \frac{C_{cv,i}}{K_{fr}} \\ &= \frac{C_{cv,i}}{\frac{1}{K_{lang}\omega_{max}}} \\ &= K_{lang}\omega_{max}C_{cv,i} \end{aligned} \tag{39}$$

Typically, these assumptions are valid in full-scale conditions, so both isotherms should yield similar results. The Figure 24 verifies this analysis. The parameters used in this model were taken from the full-scale values reported in the Pleasant Prairie study [8].

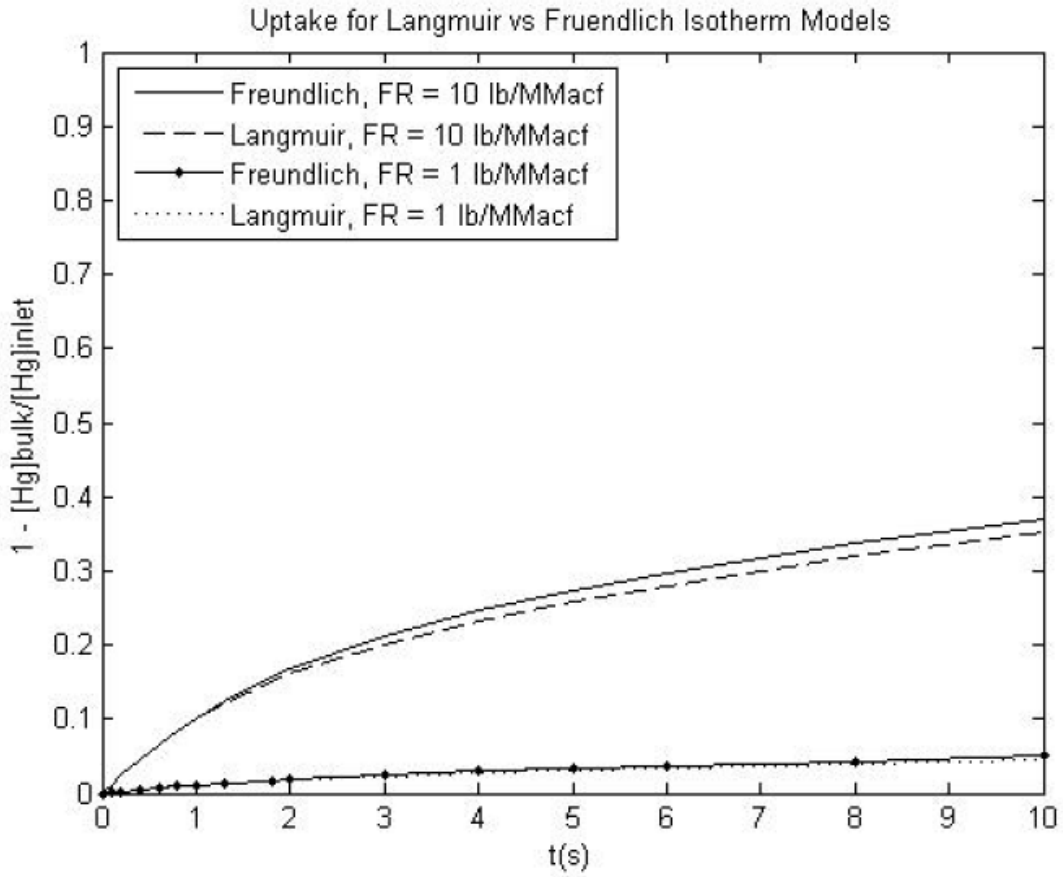

Figure 24 Mercury uptake normalized with inlet concentration over time using the Freundlich and Langmuir isotherm models. These results used “bined” activated carbon as described by Cremer et al. [8] (Kfr=1/Klang□max=0.0149).

Intraparticle Diffusion

As shown in Figures 15 and 17, intraparticle diffusion can be observed at short residence times in varying degrees. The concentration gradient inside the particle largely depends on the size of the particle itself. At a diameter of 30 μm as shown in the previous figures, mercury cannot diffuse to the center of the particle in short residence times if the solid and gas phases remain in equilibrium. However, when particle diameter is decreased to 5 μm, mercury has a shorter distance to travel and the concentration gradients are more apparent as shown in Figure 25.

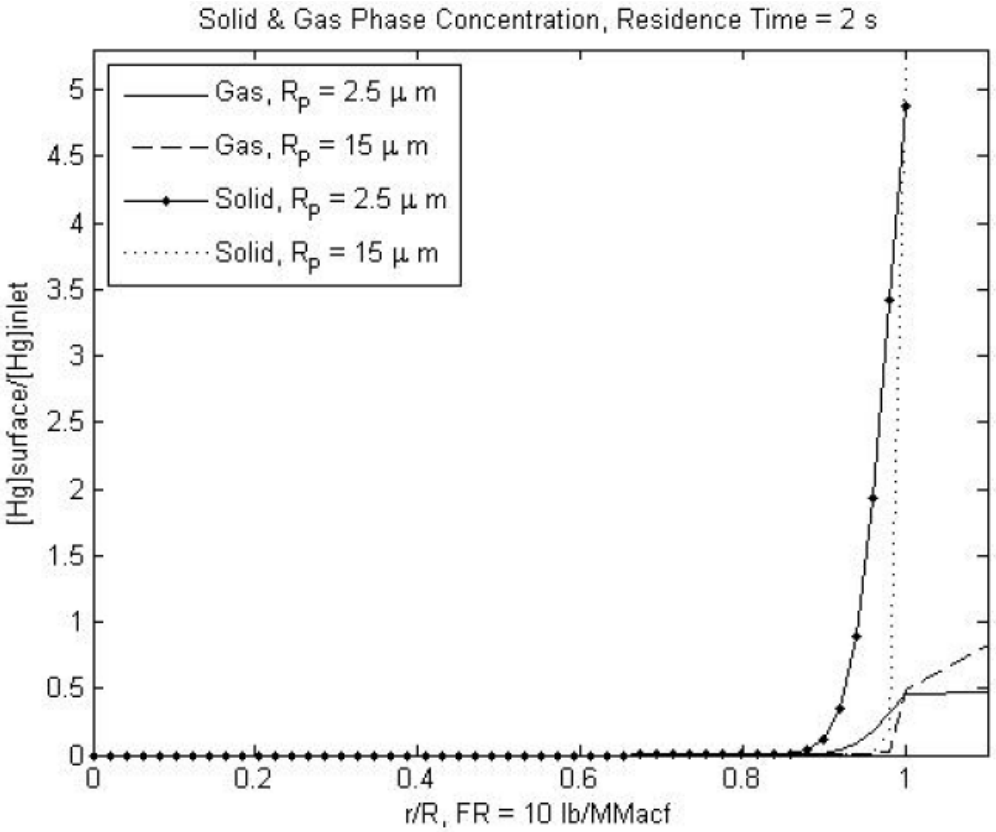

Figure 25 Comparison of gas and solid phase mercury concentration normalized with the inlet concentration inside the particle using the Freundlich adsorption model using different particles diameters.

The Langmuir isotherm adsorption model shows an even more dramatic gradient change when particle size is decreased as shown in Figure 26.

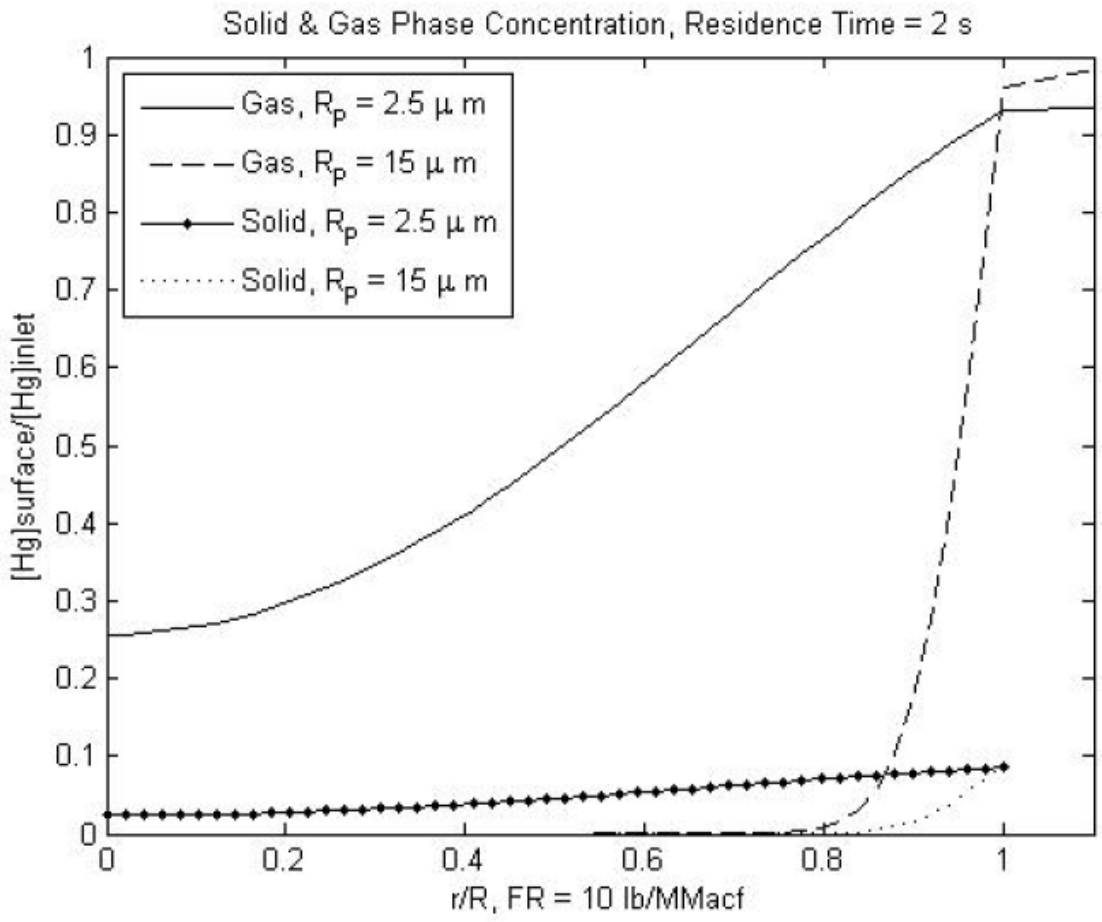

Figure 26 Comparison of gas and solid phase mercury concentration normalized with the inlet concentration inside the particle using the Langmuir adsorption model using different particles diameters.

Explanation of Wall Effects

The uptake results for the binned particles in Figure 20 are lower than that seen in the full-scale results shown in Figure 27. If a 25% correction is added to the uptake shown in Figure 21, the full-scale data may be more closely simulated as shown in Figure 28. Admittedly, this correction factor is highly qualitative, but it does allow for a predictive capacity that comes within 10% of full-scale values reported by Cremer et al. [8] .

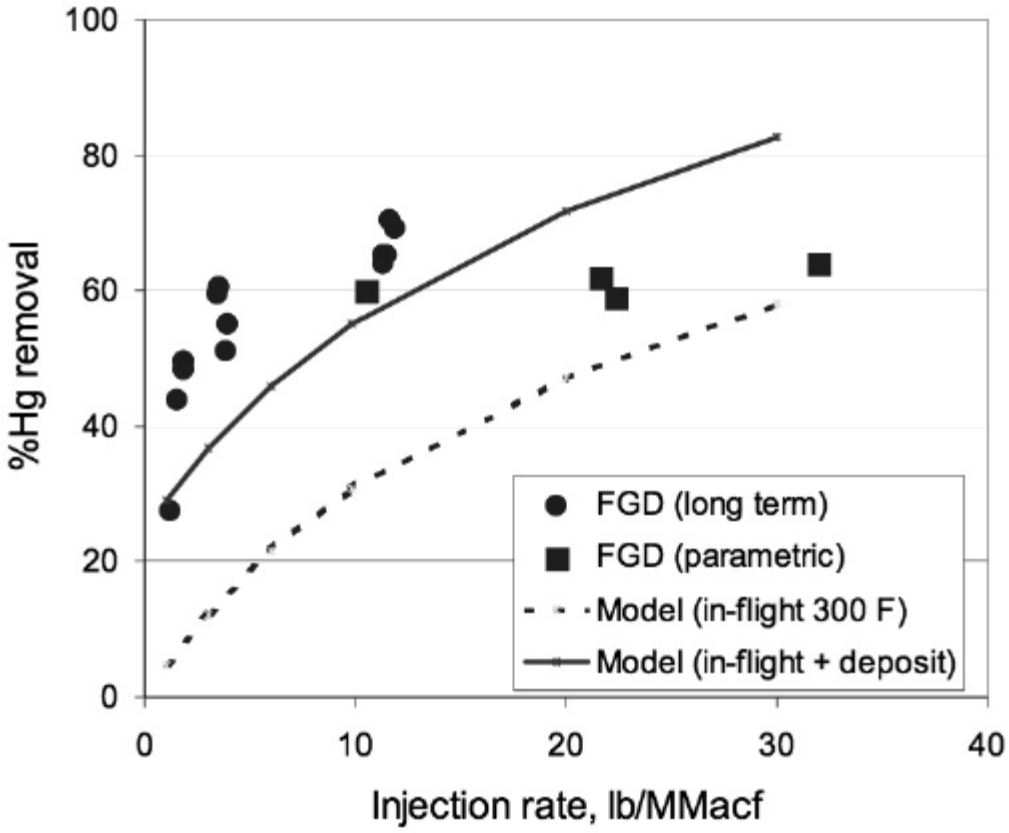

Figure 27 Full-scale mercury uptake at Pleasant Paire as reported by Cremer et al. (8)

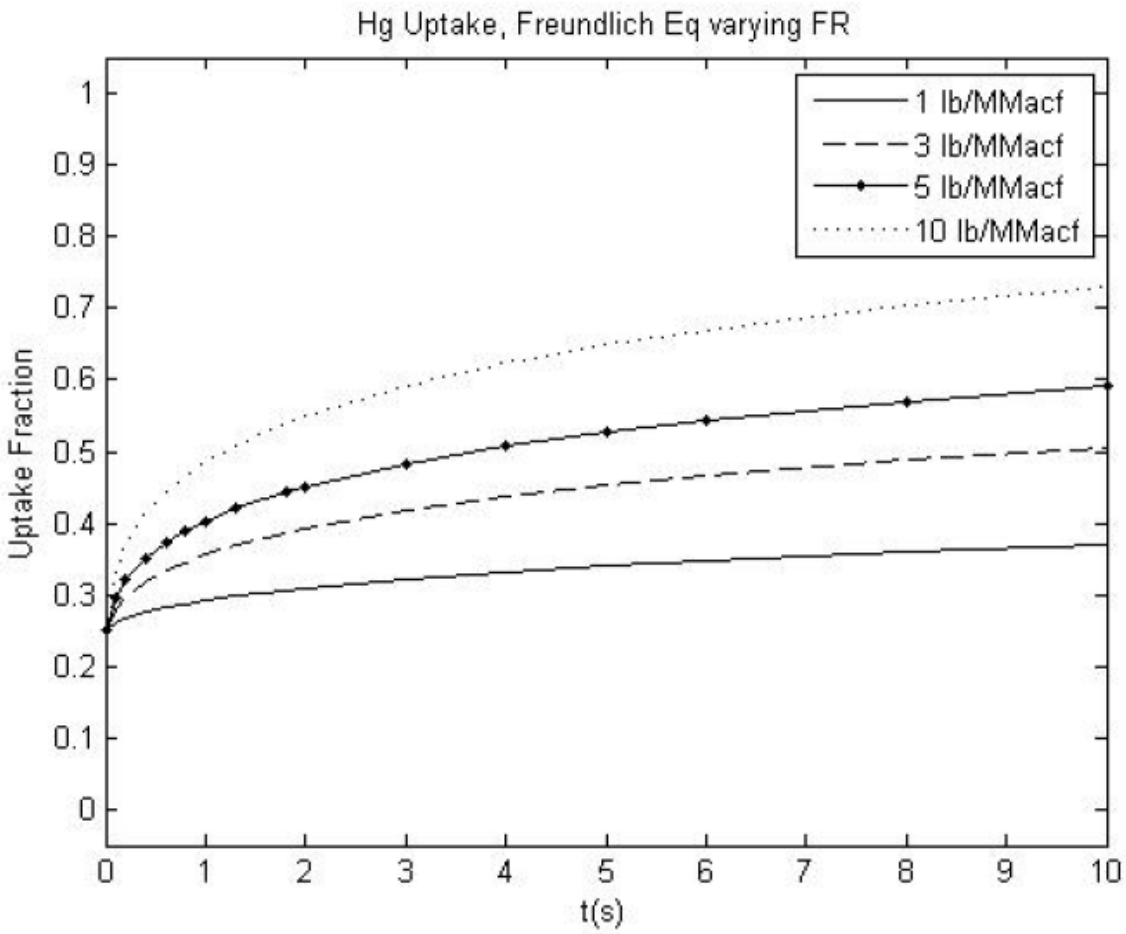

Figure 28 Mercury uptake using Freundlich isotherm adsorption model. The particles are “binned” and a 25 % correction factor is added to simulate “wall effects”.

Figure 29 shows results that may be directly compared to Figure 27. The solid line represents a 25% total uptake correction as shown in Figure 28 while the dotted line shows uptake that is 66% in-flight and 33% wall effect. The basic 25% correction seems to match the full scale data more closely, which points to the conclusion that the "packed bed" that forms on the wall of the duct likely does so quickly and does not change throughout the duration of the test.

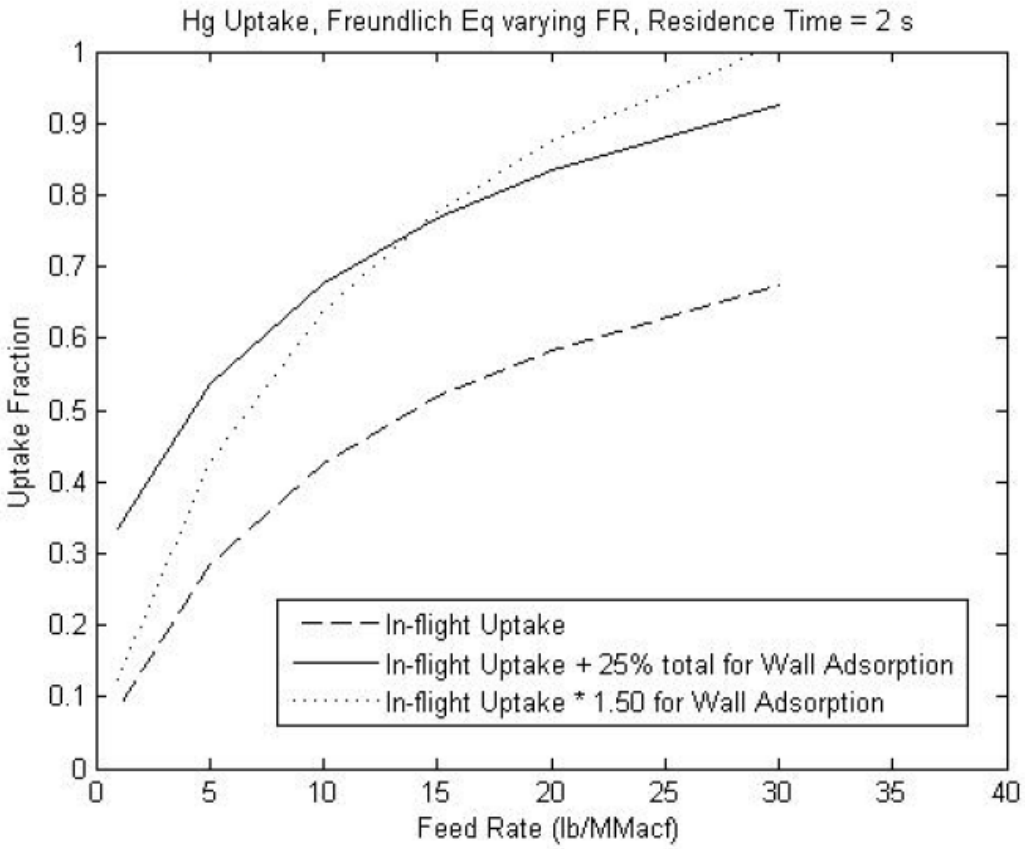

Figure 29 Mercury uptake normalized with inlet concentration inside the particle using the Freundlich isotherm adsorption model . The particles are “binned”, and a total uptake 25% or 50% proportional uptake increase is added as a correction factor to simulate “wall effects”.

CONCLUSIONS

- The experimental setup does not allow the use of powdered activated carbons as sorbents due to the high pressure drop across the fixed-bed reactor.

- Classical breakthrough curves were not observed with the coconut-shell activated carbon under the periods of time and flue gas compositions considered in this report because of the large sample size.

- Without halogen species, the coconut-shell activated carbon provided negligible mercury capture at 150^{o}C. Under these conditions the sorbent is not effective for mercury capture.

- The highest efficiency of the sorbent for mercury capture, near 100 percent, was obtained upon exposure of the coconut-shell carbon either to 50 ppm chlorine (as HCl equivalent) or 50 ppm bromine (as HBr equivalent) at 150^{o}C.

- When the carbon was exposed to 100 ppm SO_2 in the absence of halogens, the sorbent adsorption efficiency increased from 20 percent to 30 percent. When 50 ppm chlorine (as HCl equivalent) was added to the flue gas after the addition of SO_2 at concentrations ranging from 100 ppm to 500 ppm, the adsorption efficiency increased. In contrast, when the SO_2 was added at concentrations ranging from 100 ppm to 500 ppm after the addition of 50 ppm HCl, the sorbent adsorption capacity decreased. The extent of this decrease was proportional to the SO_2 concentration. This reduction was not observed when the HCl concentration increased to 100 ppm.

- In presence of 50 ppm bromine (as HBr equivalent) almost 100% adsorption was observed, the extent of this adsorption was not significantly affected by the addition of HCl or SO_2.

- The Langmuir-based, fixed-bed model shows a reasonable ability to fit fixed-bed breakthrough data from a variety of sources for powdered activated carbons.

- Wall effects are extremely important in entrained particle models. They can account for as much as 50 percent of removal perceived to be “in-flight”. As of yet, the wall effects cannot be quantitatively modeled, but enough is known about them to generate a qualitative correction factor that can place mercury uptake predictions within 10 percent or 20 percent of full-scale tests. As more full-scale data is complied and reported, this correction factor may be improved.

- Several options exist for solid-phase adsorption models. An adsorption/desorption rate model was insufficient in predicting full-scale entrained mercury capture. Freundlich and Langmuir isotherm models are both mathematically adequate.

- It is important to include the particle size distribution, in this study as bins of particles. Uptake is strongly related to particle size. Furthermore, intraparticle diffusion was found to offer significant resistance to adsorption for larger particles.

Acknowledgement

This material is based upon work supported by the Department of Energy under Award Number DE-FC26-06NT42808.

LIST OF FIGURES

Figure 1 Elemental (Hg^0) and total (Hg^T) mercury concentrations at the exit of the carbon bed as a function of time (hours) at a temperature of 150^oC at HCl concentration of 50 ppm and SO_2 concentrations ranging from 100 to 500 ppm.

Figure 2 Elemental (Hg^0) and total (Hg^T) mercury concentrations at the exit of the carbon bed as a function of time (hours) at a temperature of 150^oC at HCl concentration of 100 ppm HCl andSO_2 concentrations of 500 ppm, 100 ppm and 300 ppm.

Figure 3 Elemental (Hg^0) and total (Hg^T) mercury concentrations at the exit of the carbon bed as a function of time (hours) at a temperature of 150^oC at SO_2 concentrations of 100, 200, 500 ppm and HCl concentration of 50 ppm.

Figure 4 Elemental (Hg^0) and total (Hg^T) mercury concentrations at the exit of the carbon bed as a function of time (hours) at a temperature of 150^oC at a bromine concentration of 35.28 ppm (as HBr equivalent) and 50 ppm HCl.

Figure 5 Elemental (Hg^0) and total (Hg^T) mercury concentrations at the exit of the carbon bed as a function of time (hours) at a temperature of 150^oC at a bromine concentration of 35.28 ppm (as HBr equivalent) , HCl concentration of 50 ppm and SO_2 concentration of 500 ppm.

Figure 6 Elemental (Hg^0) and total (Hg^T) mercury concentrations at the exit of the carbon bed as a function of time (hours) at a temperature of 150^oC at NO_2 concentrations of 5 and 20 ppm NO_2.

Figure 7 Breakthrough curves for fly ash with a bed temperature of 150^oC. (A) Initial mercury concentration, C_o=2.8 mg/m^3, (B) C_o=10mg/m^3. Experimental data

o from Karatza et al [3]. , Calculated values obtained with the heterogeneous model.

Figure 8 Breakthrough curves lignite activated carbon with a bed temperature of 107°C. (A) Mercury and baseline gases, (B) Mercury, 50 ppm HCl and baseline gases. Experimental data o from Miller et al [4]. , Calculated data obtained with the heterogeneous model.

Figure 9 Breakthrough curves lignite activated carbon with a bed temperature of 107°C. (A) Mercury, 1600 ppm SO_2 and baseline gases, (B) Mercury, 20 ppm NO_2 and baseline gases. Experimental data from Miller et al [4], Calculated data obtained with the heterogeneous model.

Figure 10 The basic mass balance scheme used in a shell inside a uniform, spherical sorbent particle.
Figure 11 The organization of the discretization scheme used in the author's model.

Figure 12 Mercury uptake normalized with inlet concentration over time using the rate model.

Figure 13 Mercury uptake normalized with inlet concentration in both the solid and gas phases using the rate model.

Figure 14 Mercury uptake normalized with inlet concentration over time using the Langmuir isotherm model.

Figure 15 Mercury concentration normalized with inlet concentration inside the sorbent particle using Langmuir isotherm model.

Figure 16 Mercury uptake normalized with inlet concentration over time using Freundlich isotherm model.

Figure 17 Mercury uptake normalized with inlet concentration over time using Freundlich isotherm model.

Figure 18 Mercury uptake normalized with inlet concentration over time using Freundlich isotherm model and varying particle diameter.

Figure 19 One example of how activated carbon particles may be distributed in "bin" form.

Figure 20 A comparison of uptake for "binned" and "nonbinned" particle sets for two different feed rates. "Binned" at size range from 2 μm to 75 μm and averaging 30 μm which is the size angle used in the "nonbinned" model.

Figure 21 A comparison of uptake for “binned” and “nonbinned” particle sets for two different feed rates. “Binned” at size range from 2 μm to 75 μm and averaging 30 μm which is the size angle used in the “nonbinned” model.

Figure 22 Mercury uptake normalized with inlet concentration over time using the Freundlich isotherm model and varying the feed rate (R_p=15 μm).

Figure 23 Mercury uptake normalized with inlet concentration over time using the Freundlich isotherm model and maximizing Dab to minimize resistance from external mass transfer (R_p=15μm).

Figure 24 Mercury uptake normalized with inlet concentration over time using the Freundlich and Langmuir isotherm models. These results used “bined” activated carbon as described by Cremer et al. [8] ($K_{fr}=1/K_{lang}\omega_{max}$=0.0149).

Figure 25 Comparison of gas and solid phase mercury concentration normalized with the inlet concentration inside the particle using the Freundlich adsorption model using different particles diameters.

Figure 26 Comparison of gas and solid phase mercury concentration normalized with the inlet concentration inside the particle using the Langmuir adsorption model using different particles diameters.

Figure 27 Full-scale mercury uptake at Pleasant Paire as reported by Cremer et al. [8]

Figure 28 Mercury uptake using Freundlich isotherm adsorption model. The particles are “binned” and a 25 % correction factor is added to simulate “wall effects”.

Figure 29 Mercury uptake normalized with inlet concentration inside the particle using the Freundlich isotherm adsorption model . The particles are “binned”, and a total uptake 25% or 50% proportional uptake increase is added as a correction factor to simulate “wall effects”.

REFERENCES

(1) Fry, A., Cauch, B., Silcox, G., Lighty, J., Senior, C. *Proceedings of the Combustion Institute* **2007**, 31, 2855-2861.

(2) Schaeffer K., Potwora, R. Coconut Shell versus Bituminous Coal Activated carbon. June 2008. Carbon Resources.

(3) Karatza, D., Lancia, A., Musmarra, D. *Environ. Sci. Technol.* **1998**, 32, 3999-4004.

(4) Miller, S., Dunham, G., Olson, E., Brown, T. *Fuel Processing Technology* **2000,** 65-66, 343-363.

(5) Gardner, P.J., Pang, P., Preston, S.R. *J. Chem. Eng. Data* **1991**, 36, 265-268.
(6) Massman, W.J. *Atmospheric Environment* **1991,** 33, 453-457.
(7) Bird, S., Lightfoot, *Transport phenomena,* 2nd ed.; WILEY-VCH, 2000.
(8) Cremer, M., Senior, C., Chiodo, A., Wang, D., Valentine, J. *CFD Modeling of Activated Carbon Injection for Mercury Control in Coal-Fired Power Plants.* Technical report, 2005.
(9) McCabe, W., Smith, J., Harriot, P.P. *Unit Operations of Chemical Engineering.* McGraw Hill Inc., 1993.
(10) Scala, F. *Envirionmental Science & Technology.***2001**, 35, 4367-4372.
(11) Scala, F. *Industrial & Engineering Chemistry Research* **2004,** 43, 2575-2589.
(12) Flora, J.R.V., Hargis, R. A., O'Dowd, W.J., Pennline, H.W., Vidic, R.D. *J. Air & waste Manage. Assoc.* **2003,** 53, 478-488.
(13) Bustard, J., Durham, M., Starns, T., Lindsey, C.,Martin, C., Schlager, R., Baldrey, K. *Fuel Processing Technology* **2004**, 85, 549-562.
(14) Pollack, N.R. *Sorbent Injection: taking the technology from R&D to Comercial Launch.* Technical Report, 2008.
(15) Meserole, F.B., Change, R.,Carey, T.R., Machac, J., Richardson, C.F. *J. Air & Waste manage. Assoc.* **1999**, 19, 694-704.

ABBREVIATIONS

g/g:	Grams of Mercury per Grams of Carbon
g Hg/m^3:	Grams of Mercury per Cubic Meter
$\mu g/m^3$:	Micrograms per Cubic Meter
μm:	Micrometers
nm:	Nanometers
m^3/g min:	Cubic meter per gram per minute
min^{-1}:	1/minute
mg/m^3:	Milligram per Cubic Meter
C:	Celsius
Co:	initial Mercury Concentration
cm:	Centimeters
CO:	Carbon Monoxide
CO_2:	Carbon Dioxide
F:	Fahrenheit
g;	Grams
HCl:	Hydrochloric Acid
HBr:	Hydrogen Bromide
Hg:	Mercury
$HgCl_2$:	Mercuric Chloride
Hg^o:	Elemental Mercury
Hg^T:	Total Mercury
H_2O:	Water

ID:	Internal Diameter
K:	Kelvin
lb:	Pounds
m:	meters
m^2:	Square Meters
m^3:	Cubic Meter
mg:	Milligrams
min:	Minutes
mm:	Millimeters
N_2:	Nitrogen
NO:	Nitrogen Monoxide
NO_2:	Nitrogen Dioxide
O_2:	Oxygen
OD:	Outer Diameter
ppm:	Parts Per Million
ppmv:	Parts Per Million by Volume
s:	Seconds
SLPM:	Standard Liters per Minute
$SnCl_2$:	Stannous Chloride
SO_2:	Sulfur Dioxide
W:	Watts